

Deeply virtual meson production at HERA and at the EIC within the Color Glass Condensate EFT

Renaud Boussarie,^a Luigi Delle Rose,^{b,c} Michael Fucilla,^d Alessandro Papa,^{b,c} Lech Szymanowski,^d Samuel Wallon,^e

^a*CPHT, CNRS, Ecole Polytechnique, Institut Polytechnique de Paris, 91128 Palaiseau, France*

^b*Dipartimento di Fisica, Università della Calabria, Arcavacata di Rende, I-87036, Cosenza, Italy*

^c*INFN, Gruppo Collegato di Cosenza, Arcavacata di Rende, I-87036, Cosenza, Italy*

^d*National Centre for Nuclear Research (NCBJ), Pasteura 7, 02-093 Warsaw, Poland*

^e*Université Paris-Saclay, CNRS/IN2P3, IJCLab, 91405, Orsay, France*

E-mail: renaud.boussarie@polytechnique.edu, luigi.dellerose@unical.it,
michael.fucilla@ncbj.gov.pl, alessandro.papa@fis.unical.it,
lech.szymanowski@ncbj.gov.pl, samuel.wallon@ijclab.in2p3.fr

ABSTRACT: Continuing our previous study of Deeply Virtual Meson Production (DVMP) at twist-3 accuracy, we derive compact expressions for all helicity amplitudes. We perform a phenomenological analysis of the helicity-amplitude ratio $\mathcal{A}^{11}/\mathcal{A}^{00}$ and of the spin-density matrix element r_{00}^{04} within the Color Glass Condensate framework. Small- x evolution is incorporated by numerically solving the running-coupling-and-collinearly-improved Balitsky–Kovchegov and Balitsky–Fadin–Kuraev–Lipatov equations with the McLerran–Venugopalan model as the initial condition. By capturing a relevant subset of next-to-leading order corrections, we provide the most theoretically accurate description of these observables to date. Our results are compared to HERA data, and predictions are presented for electron–lead collisions at the future Electron–Ion Collider. We discuss the impact of non-linear effects at low photon virtuality and the role of genuine higher-twist contributions associated with light vector meson distribution amplitudes, corresponding to higher Fock-state components of the projectile.

Contents

1	Introduction	1
2	Theoretical set-up	3
2.1	CGC effective framework	3
2.2	Kinematics, frame and polarization vectors	4
2.3	BK and BFKL evolution of the dipole operator	5
2.4	Twist-2 and -3 distribution amplitudes	6
3	Helicity amplitudes	7
3.1	Helicity amplitudes: 2-body Fock state	7
3.2	Helicity amplitudes: 3-body Fock state	9
4	Numerical results	12
4.1	Helicity amplitudes ratio and spin-density matrix element r_{00}^{04} at the HERA and the EIC	12
5	Conclusions and Outlook	15
A	Evolutions of DAs as a function of μ	17
B	Explicit parametrization of the set of DAs	19
C	Derivation of the dipole part of the 3-body amplitude	21
C.1	$\mathcal{U}_{z_1 z_2}$ -part of the amplitude	21
C.2	$\mathcal{U}_{z_1 z_3}$ plus $\mathcal{U}_{z_3 z_2}$ -part of the amplitude	24
C.3	Full result for $\mathcal{A}_3^{T,L}$ and $\mathcal{A}_3^{T,T}$	27
C.4	Summary of $F_i(x_i, x_j, \mathbf{r}^2)$ and $\tilde{F}_i(x_i, x_j, \mathbf{r}^2)$'s functions	28

1 Introduction

The exclusive production of light vector mesons in deep inelastic scattering (DIS) has played a central role in revealing the dynamics of QCD at high energies. The HERA measurements of $e^\pm p$ collisions [1–13] established that diffractive events constitute a significant fraction of the total DIS cross section, and they provided early indications of gluon saturation at small Bjorken- x [14, 15]. In this kinematic domain, the proton behaves as a dense gluonic system whose evolution can be described within the Color Glass Condensate (CGC) effective theory [16–34], a framework that captures the onset of gluon saturation and describes the small- x part of the hadronic wave function as a highly occupied, strongly fluctuating ensemble of color fields. In this picture, the target at high energy resembles a disordered color

medium, where multiple scattering and non-linear gluon recombination processes become essential, and coherent interactions with these intense gauge fields dominate the dynamics. The experimental identification of this regime is one of the most intriguing prospects for modern high-energy colliders, and constitutes a central pillar of the physics program of the future Electron–Ion Collider [35].

However, reaching quantitative accuracy within the CGC framework requires the systematic inclusion of several subdominant effects. A first and essential ingredient is the incorporation of next-to-leading order corrections, which improve the stability of the perturbative expansion and reduce the scheme and scale dependence of theoretical predictions. In particular, running-coupling contributions [36], full NLO corrections to the small- x evolution kernel [37–43] and NLO corrections to the impact factors [44–62], constitute indispensable steps toward a controlled phenomenology of dense gluonic matter. A second class of refinements involves sub-eikonal corrections [63–79], which capture $1/W^2$ -suppressed interactions, where W^2 stands for center-of-mass energy, absent in the strict eikonal limit. Finally, as highlighted in [80], since the saturation scale is not parametrically large in present and near-future experimental conditions, power-suppressed contributions proportional to inverse powers of the hard scale—*i.e.* higher-twist effects—may also induce sizeable modifications to exclusive and diffractive observables. This makes the systematic control of all these subleading contributions a prerequisite for precision phenomenology at small x .

Beyond providing precision corrections, the inclusion of higher-twist effects can significantly enlarge the set of observables that can be meaningfully accessed. An emblematic example is represented by the process which is the object of this study, the exclusive electroproduction of light vector mesons, a.k.a. Deeply Virtual Meson Production (DVMP), which involves the subprocess

$$\gamma^{(*)}(q) P(p_t) \rightarrow M(p_M) P(p'_t), \quad (1.1)$$

where $M = \{\rho, \phi, \omega\}$. This process has been extensively investigated both in forward electroproduction [81, 82] and in photoproduction at large momentum transfer [82–85] at HERA, and is known to provide access to the transverse spatial structure of the proton and to the dynamics of color-singlet exchange [86–91]. At HERA experiments [82], the complete spin-density matrix of the DVMP has been measured, providing detailed information of all helicity amplitudes. Unfortunately, from a theoretical perspective, a complete description of the spin-density matrix is a highly challenging task. At moderate energies, one could attempt to describe the process within the framework of collinear factorization [92–95]. However, collinear factorization is rigorously justified only for the twist-2 longitudinal channel, while transitions involving transversely polarized mesons at twist 3 are plagued by end point singularities [96, 97].

Various approaches, based on different theoretical ideas, have been developed to address the challenges of describing higher-twist contributions. One such approach relies on improved collinear approximations [98–102]. However, in the high-energy kinematics rele-

vant for HERA and the future EIC, a more natural description emerges from high-energy formulations [86, 103–110], where the end-point singularities are naturally regularized by non-zero transverse momenta of t -channel gluons. In this case, the gluon distribution is described in terms of momentum-space unintegrated gluon density [105, 111–116]. Especially for the EIC physics case, a very exciting perspective is the description of the exclusive diffractive meson production at high-energy, including the saturation regime. A first synthesis of these ideas at small- x was achieved in Ref. [60], where exclusive longitudinal meson production was computed at NLO within a saturation framework in terms of leading-twist DAs. In subsequent works [80, 117], the extension of this program to twist-3 observables was started, providing, at the LO, a complete description of the $\gamma^{(*)} \rightarrow M(\rho, \phi, \omega)$ impact factor, for arbitrary photon/meson polarization and in fully general kinematics, including both the genuine and the kinematic higher-twist effects.

In this paper, we initiate a phenomenological exploration of the spin-density matrix for exclusive ρ -meson leptonproduction within the novel framework proposed in [80, 117]. The paper is organized as follows. Section 2 introduces the general formalism and describes all ingredients entering the numerical analysis, *i.e.* target matrix elements and collinear distribution amplitudes parametrizations. Appendix A is devoted to the renormalization group evolution of the latter. Section 3 presents the two- and three-body helicity amplitudes. These amplitudes—derived from the original expressions in Refs. [80, 117] by employing a dipole approximation and an expansion around the forward direction—are recast into a form better suited for numerical implementation. Their derivation is lengthy and algebraically intricate, so the appendix C is entirely devoted to this calculation. Section 5 contains the numerical results, and Section 6 summarizes our findings.

2 Theoretical set-up

2.1 CGC effective framework

Throughout this work, we employ the semi-classical effective description of QCD at small x [22–25, 118–120]. For this purpose, we introduce a light-cone basis defined by two null vectors n_1 and n_2 , which specify the $+/-$ directions and satisfy $n_1 \cdot n_2 = 1$. The Sudakov decomposition of an arbitrary four-vector k reads¹

$$k^\mu = k^+ n_1^\mu + k^- n_2^\mu + k_\perp^\mu. \quad (2.1)$$

In this approach, the gluon field $\mathcal{A}(k)$ is separated into a classical background field $b(k)$, dominated by small- k^+ modes, and quantum fluctuations $A(k)$ associated with large- k^+ modes. After performing a large boost from the target rest frame to the projectile frame, the background field takes the form

$$b^\mu(x) = b^-(x^+, x_\perp) n_2^\mu = \delta(x^+) \mathbf{B}(\mathbf{x}) n_2^\mu, \quad (2.2)$$

¹Transverse momenta in Euclidean space are denoted in boldface, while Minkowskian transverse components carry a \perp subscript.

corresponding to the standard *shockwave approximation*. In this configuration, the fast projectile propagates predominantly along the n_1 (“+”) direction, while the target moves along n_2 (“−”). It is therefore convenient to work in the light-cone gauge

$$A \cdot n_2 = 0,$$

which provides the natural setting for the CGC formalism. Resumming the multiple scatterings of a fast projectile parton off the background field leads to a light-like Wilson line localized at $z^- = 0$,

$$W_z = \mathcal{P} \exp \left(ig \int dz^+ b^{-a}(z) \mathbf{T}_r^a \right), \quad (2.3)$$

where \mathcal{P} denotes path ordering along the + direction and \mathbf{T}_r^a is the color generator in the representation r . In the following, V_z and U_z denote Wilson lines in the fundamental ($\mathbf{T}_r^a \rightarrow t_{ij}^a$) and adjoint ($\mathbf{T}_r^a \rightarrow -if^{abc}$) representations, respectively. Within the CGC formalism, the scattering amplitude is expressed as the convolution of a perturbatively calculable projectile impact factor with a non-perturbative target matrix element built from Wilson-line operators evaluated between proton (or nuclear) states.

2.2 Kinematics, frame and polarization vectors

We denote by q the four-momentum of the incoming photon and by p_t the four-momentum of the target proton. The photon momentum admits the Sudakov decomposition

$$q^\mu = q^+ n_1^\mu - \frac{Q^2 - \mathbf{q}^2}{2q^+} n_2^\mu + q_\perp^\mu. \quad (2.4)$$

The produced meson momentum can be written as

$$p_M^\mu = p_M^+ n_1^\mu + \frac{\mathbf{p}_M^2 + m_M^2}{2p_M^+} n_2^\mu + p_{M\perp}^\mu. \quad (2.5)$$

Conversely, the target proton moves ultra-relativistically in the opposite direction with a dominant − component,

$$p_t^\mu = p_t^- n_2^\mu, \quad (2.6)$$

where its mass has been neglected and we have chosen $p_{t\perp} = 0_\perp$. In the high-energy limit we use

$$s = (q + p_t)^2 = (p_M + p_t')^2 \simeq 2q \cdot p_t = 2p_M \cdot p_t'. \quad (2.7)$$

After the interaction, the outgoing proton acquires a transverse momentum,

$$p_t'^\mu = p_t^- n_2^\mu + \Delta_\perp^\mu = p_t^- n_2^\mu + q_\perp^\mu - p_{M\perp}^\mu. \quad (2.8)$$

The amplitudes derived in [117] were obtained in the general frame described above. For the purposes of the present analysis, however, it is convenient to adopt a less general frame², in which the incoming photon carries no transverse momentum in the Sudakov sense:

$$q_\perp = 0_\perp, \quad \Delta_\perp = -p_{M\perp}. \quad (2.9)$$

²Throughout the paper, we keep the derivation fully general; however, the final expressions for the amplitudes used in the numerical implementation are presented in this specific frame.

In this frame, the polarization vectors are chosen according to the experimental convention of [121], also adopted in Ref. [105]. The photon polarization vectors read

$$\varepsilon_{\gamma L}^\mu = \frac{1}{Q} \left(q^\mu + \frac{2Q^2}{s} p_t^\mu \right), \quad \varepsilon_{\gamma T}^{(\pm)} = \varepsilon_{\gamma \perp}^{(\pm)} = \frac{1}{\sqrt{2}} (0, \mp 1, -i, 0) \equiv (0, \varepsilon_\gamma^{(\pm)}, 0). \quad (2.10)$$

The meson polarization vectors are defined as

$$\varepsilon_{ML}^\mu = \frac{1}{m_M} \left(p_M^\mu - \frac{2m_M^2}{s} p_{t'}^\mu \right), \quad \varepsilon_{MT}^{(\pm)\mu} = \varepsilon_{M\perp}^{(\pm)\mu} - \frac{\varepsilon_{M\perp}^{(\pm)} \cdot p_{M\perp}}{p_M^+} n_2^\mu, \quad (2.11)$$

with

$$\varepsilon_{M\perp}^{(\pm)} = \frac{1}{\sqrt{2}} (0, \mp 1, -i, 0) \equiv (0, \varepsilon_M^{(\pm)}, 0). \quad (2.12)$$

Since we are not in strictly forward kinematics with $\Delta_\perp = 0$, the transverse polarization vector of the meson is not purely transverse in the Sudakov sense. However, the induced non-transverse component does not contribute to the scattering amplitude. The transverse polarization vectors of the photon and meson satisfy the orthonormality relations

$$\varepsilon_\gamma^{(+)} \cdot \varepsilon_M^{(+)*} = \varepsilon_\gamma^{(-)} \cdot \varepsilon_M^{(-)*} = 1, \quad \varepsilon_\gamma^{(-)} \cdot \varepsilon_M^{(+)*} = \varepsilon_\gamma^{(+)} \cdot \varepsilon_M^{(-)*} = 0. \quad (2.13)$$

2.3 BK and BFKL evolution of the dipole operator

In this section, we describe the parametrization of the target matrix element and its small- x evolution under the non-linear BK equation. Our definition of the forward dipole matrix element, at rapidity separation η , is

$$\mathcal{U}(\mathbf{r}, \eta) = \lim_{p_t^- \rightarrow p_t} \frac{\langle P(p_{t'}) | \mathcal{U}_{\mathbf{r}, \mathbf{0}}^\eta | P(p_t) \rangle}{2p_t^- (2\pi) \delta(p_{t'}^- - p_t^-) (2\pi)^2 \delta^2(\mathbf{p}_{t'} - \mathbf{p}_t)}, \quad (2.14)$$

where the dipole operator is defined as

$$\mathcal{U}_{z_1, z_2}^\eta = 1 - \frac{1}{N_c} \text{tr} \left(V_{z_1}^\eta V_{z_2}^{\eta\dagger} \right). \quad (2.15)$$

For the parametrization of the non-perturbative target correlator at the initial condition $\eta = 0$, we use the McLerran-Venugopalan model [118–120]

$$\mathcal{U}(\mathbf{r}, \eta = 0) \equiv \mathcal{U}(r, \eta = 0) = 1 - \exp^{-\frac{r^2 Q_0^2}{4} \ln\left(\frac{1}{r\Lambda} + e\right)}, \quad (2.16)$$

with $\Lambda = 0.241$ GeV, e the Euler constant and $r = |\mathbf{r}|$. The parameter Q_0^2 is chosen as $Q_0^2 = 0.104$ GeV² for a proton target, and as $Q_0^2 = 6 \times 0.104$ GeV² for a large nucleus, where the factor 6 corresponds to the geometric scaling factor $A^{1/3}$ for a lead target.

We implement the evolution of the dipole operator, including running-coupling effects, exactly as in [122], *i.e.* following the derivation of Ref. [123]. For completeness, we reproduce below the form of the equation implemented in our numerical analysis,

$$\frac{\partial \mathcal{U}(r, \eta)}{\partial \eta} = \int d\phi dr_z r_z \left[\frac{\bar{\alpha}_s(r)}{2\pi r_z^2} \left(\frac{r^2}{r_{zy}^2 + \epsilon^2} + \frac{\bar{\alpha}_s(r_z)}{\bar{\alpha}_s(r_{zy})} - 1 + \frac{r_z^2}{r_{zy}^2 + \epsilon^2} \left(\frac{\bar{\alpha}_s(r_{zy})}{\bar{\alpha}_s(r_z)} - 1 \right) \right) \right]$$

$$\times \left[\mathcal{U}(r_z, \eta - \delta_{r_z;r}) + \mathcal{U}(r_{zy}, \eta - \delta_{r_{zy};r}) - \mathcal{U}(r, \eta) - \xi \mathcal{U}(r_z, \eta - \delta_{r_z;r}) \mathcal{U}(r_{zy}, \eta - \delta_{r_{zy};r}) \right], \quad (2.17)$$

where

$$r_{zy} = \sqrt{r^2 + r_z^2 - 2rr_z \cos \phi},$$

$$\delta_{r_z;r} = \max \left\{ 0, 2 \ln \left(\frac{r}{r_z} \right) \right\}, \quad \delta_{r_{zy};r} = \max \left\{ 0, 2 \ln \left(\frac{r}{r_{zy}} \right) \right\}.$$

The prescription for $\bar{\alpha}_s$ is the one introduced in Ref. [124] and quoted in eqs. (5) and (6) of [122]. We emphasize that the only difference with respect to the implementation of [122] is that we write the evolution in terms of the dipole operator $\mathcal{U}(r, \eta) = 1 - S(r, \eta)$, whereas they formulate it in terms of $S(r, \eta)$. Furthermore, we introduce a parameter ξ that allows us to switch from the non-linear BK equation ($\xi = 1$) to the linear BFKL limit ($\xi = 0$). We validated our implementation by comparing the $\xi = 1$ case with the results of [122], finding agreement at the permille level. In the following, for simplicity of notation, we write $\mathcal{U}(r, \eta) \equiv \mathcal{U}(r)$.

2.4 Twist-2 and -3 distribution amplitudes

The additional non-perturbative ingredients required in our analysis are the explicit parametrizations of the higher-twist collinear distribution amplitudes (DAs). These were originally derived in Ref. [125]. In addition to their asymptotic forms, we implement their renormalization-group evolution. The scale dependence of the DAs enters their expressions below through the coupling constants $a_2(\mu^2)$, $\omega_{\{1,0\}}^A(\mu^2)$, $f_{3M}^A(\mu^2)$, and $f_{3M}^V(\mu^2)$, whose evolution equations are given in Ref. [125]. For the convenience of the reader, Appendix A collects both the evolution equations and the values of these constants for the ρ meson ($M = \rho$) at $\mu^2 = 1$ GeV², which are used in our numerical analysis. In this analysis, we take the ρ meson mass to be $m_\rho = 0.776$ GeV and the vector decay constant $f_\rho = 200$ MeV [126].

Distribution amplitudes parametrization. The longitudinal meson DA is parameterized as [104]

$$\varphi_{\parallel}(z) = 6z(1-z) \left(1 + \frac{3}{2} a_2(\mu^2) (5(2z-1)^2 - 1) \right). \quad (2.18)$$

The genuine twist-3 DAs, in terms of which the results of Ref. [117] can be expressed, read [104]

$$V(x_1, x_2) = 5040 x_1 x_2 (x_1 - x_2) (1 - x_1 - x_2)^2, \quad (2.19)$$

$$A(x_1, x_2) = 360 x_1 x_2 \left(1 + \frac{\omega_{\{1,0\}}^A(\mu^2)}{2} (4 - 7(x_1 + x_2)) \right) (1 - x_1 - x_2)^2. \quad (2.20)$$

In Ref. [117], the 2-body twist-3 corrections are expressed in terms of the DAs

$$\varphi_1^T(z) \equiv \varphi_1^T(z)|_{\text{W.W.}} + \varphi_1^T(z)|_{\text{G.T.}} = -h(z) + \tilde{h}(z), \quad (2.21)$$

$$\varphi_A^T(z) \equiv \varphi_A^T(z)|_{\text{W.W.}} + \varphi_A^T(z)|_{\text{G.T.}} = -\frac{g_{\perp}^{(a)}(z)}{4} + \frac{\tilde{g}_{\perp}^{(a)}(z)}{4}, \quad (2.22)$$

where W.W. (G.T.) denotes the Wandzura–Wilczek (genuine twist-3) component of the DA. The final equalities in both expressions are given for easier comparison with the formulas of Ref. [117].

The four contributions in eqs. (2.21) and (2.22) can be expressed in terms of the independent set of DAs $\{\varphi_{\parallel}, V, A\}$, parametrized in eqs. (2.18), (2.19), and (2.20). The derivation of the explicit parameterizations of contributions in eqs. (2.21) and (2.22) is long, we relegate it to the Appendix B. We obtain

$$\varphi_1^T(z)|_{\text{W.W.}} = \frac{3}{2}z(2z^2 - 3z + 1) \left(1 + a_2(\mu^2)(1 + 15z(z - 1)) \right), \quad (2.23)$$

$$\begin{aligned} \varphi_1^T(z)|_{\text{G.T.}} = & -\frac{5}{8}z(2z^2 - 3z + 1) \left[\left(3\omega_{\{1,0\}}^A(\mu^2)(7z^2 - 7z + 1) - 16 \right) \frac{f_{3M}^A}{f_M} \right. \\ & \left. - 84(23z^2 - 23z + 1) \frac{f_{3M}^V}{f_M} \right], \end{aligned} \quad (2.24)$$

$$\varphi_A^T(z)|_{\text{W.W.}} = \frac{3}{2}z(z - 1) \left(1 + a_2(\mu^2)(1 + 5(z - 1)z) \right), \quad (2.25)$$

$$\begin{aligned} \varphi_A^T(z)|_{\text{G.T.}} = & \frac{5}{8}z(1 - z) \left[\left(\omega_{\{1,0\}}^A(\mu^2)(63z^2 - 63z + 3) - 16(14z^2 - 14z + 1) \right) \frac{f_{3M}^A}{f_M} \right. \\ & \left. - 84(5z^2 - 5z + 1) \frac{f_{3M}^V}{f_M} \right]. \end{aligned} \quad (2.26)$$

3 Helicity amplitudes

In this section, we present the final analytic form of all helicity amplitudes of the unpolarized DVMP. We distinguish contributions arising from the quark-antiquark (2-body) Fock state, which dominates at leading twist, from those involving the quark-antiquark-gluon (3-body) configurations, relevant at twist-3 accuracy. For the sake of generality, we will consider the matrix element $\mathcal{U}(\mathbf{r})$ in full generality in this section, although we will use the parametrization (2.16) in the numerical analysis.

3.1 Helicity amplitudes: 2-body Fock state

When only the leading quark-antiquark Fock state is taken into account, the small- x amplitude can be written in the dipole form

$$\mathcal{A}_2^{\lambda_V, \lambda_\gamma} = (2\pi)^4 \delta^{(4)}(q + p_t - p_M - p_{t'}) W^2 \int d^2\mathbf{r} \mathcal{U}(\mathbf{r}) \int_0^1 dz e^{iz\mathbf{\Delta}\cdot\mathbf{r}} \psi_2^{\lambda_V, \lambda_\gamma}(z, \mathbf{r}), \quad (3.1)$$

where $\lambda_\gamma = \{T, L\}$ and $\lambda_V = \{T, L\}$ represent the incoming photon and outgoing meson helicities, respectively. In the frame in which the incoming photon has no transverse momentum in the Sudakov sense, the coordinate-space impact factors for the different helicity

amplitudes read [60, 117]

$$\psi_2^{L,L}(z, \mathbf{r}) = \frac{e_q m_M f_M}{2\pi} 2z\bar{z}Q^2 K_0\left(\sqrt{z\bar{z}Q^2 r^2}\right) \left[\frac{\varepsilon_{\gamma L}^+ \varepsilon_{ML}^{+*}}{q^+ p_M^+} \right] \varphi_{\parallel}(z), \quad (3.2)$$

$$\psi_2^{L,T}(z, \mathbf{r}) = \frac{e_q m_M f_M}{2\pi} (2z-1) \sqrt{\frac{z\bar{z}Q^2}{r^2}} K_1\left(\sqrt{z\bar{z}Q^2 r^2}\right) \left[i \frac{\varepsilon_{ML}^{+*}}{p_M^+} (\mathbf{r} \cdot \boldsymbol{\varepsilon}_{\gamma}) \right] \varphi_{\parallel}(z), \quad (3.3)$$

$$\psi_2^{T,L}(z, \mathbf{r}) = \frac{e_q m_M f_M}{2\pi} 2z\bar{z}Q^2 K_0\left(\sqrt{z\bar{z}Q^2 r^2}\right) \left[i \frac{\varepsilon_{\gamma L}^+}{q^+} (\mathbf{r} \cdot \boldsymbol{\varepsilon}_M^*) \right] \varphi_1^T(z), \quad (3.4)$$

$$\begin{aligned} \psi_2^{T,T}(z, \mathbf{r}) &= -\frac{e_q m_M f_M}{2\pi} \sqrt{z\bar{z}Q^2 r^2} K_1\left(\sqrt{z\bar{z}Q^2 r^2}\right) \left[\frac{T_{\text{n.f.}}}{2} \phi_{2,\text{n.f.}}(z) + T_{\text{f.}}(\mathbf{r}) \phi_{2,\text{f.}}(z) \right] \\ &\equiv \psi_{2,\text{n.f.}}^{T,T} + \psi_{2,\text{f.}}^{T,T}, \end{aligned} \quad (3.5)$$

where we introduced the flip (f.) and non-flip (n.f.) helicity structures

$$T_{\text{f.}}(\mathbf{r}) = \frac{(\boldsymbol{\varepsilon}_{\gamma} \cdot \mathbf{r})(\boldsymbol{\varepsilon}_M^* \cdot \mathbf{r})}{r^2} - \frac{\boldsymbol{\varepsilon}_{\gamma} \cdot \boldsymbol{\varepsilon}_M^*}{2}, \quad T_{\text{n.f.}} = \boldsymbol{\varepsilon}_{\gamma} \cdot \boldsymbol{\varepsilon}_M^*, \quad (3.6)$$

and the combination of DAs

$$\phi_{2,\text{f.}}(z) = -(2z-1)\varphi_1^T(z) + \varphi_A^T(z), \quad (3.7)$$

$$\phi_{2,\text{n.f.}}(z) = -(2z-1)\varphi_1^T(z) - \varphi_A^T(z). \quad (3.8)$$

At the level of Wandzura-Wilczek approximation, it is enough to take the W.W. part of the DAs in eqs. (2.21, 2.22), while in a fully consistent twist-3 treatment, also the G.T. part must be included. The helicity structures are such that

$$T_{\text{f.}}^{(+)(+)} = T_{\text{f.}}^{(-)(-)} = 0, \quad T_{\text{f.}}^{(-)(+)} = \left(T_{\text{f.}}^{(+)(-)}\right)^* = -\frac{1}{2}e^{2i\varphi}, \quad (3.9)$$

$$T_{\text{n.f.}}^{(+)(+)} = T_{\text{n.f.}}^{(-)(-)} = 1, \quad T_{\text{n.f.}}^{(-)(+)} = \left(T_{\text{n.f.}}^{(+)(-)}\right)^* = 0, \quad (3.10)$$

where φ is the polar angle of \mathbf{r} with respect to the x axis.

Let us analyze the scaling behaviour of the different helicity amplitudes. In the following, we will use λ_{γ} (or λ_V) = 0 for longitudinal polarization, λ_{γ} (or λ_V) = 1 for “plus” ($\varepsilon^{(+)}$) transverse polarization and λ_{γ} (or λ_V) = -1 for “minus” ($\varepsilon^{(-)}$) transverse polarization. The longitudinal-photon-to-longitudinal-meson amplitude is non-zero in the forward limit and scales for $Q \rightarrow \infty$ as

$$\mathcal{A}_2^{0,0} \sim Q \int dr r K_0\left(\sqrt{z\bar{z}Q^2 r^2}\right) \sim \frac{1}{Q}, \quad (3.11)$$

thus being leading twist. The transverse-photon-to-transverse-meson s -channel helicity-conserving (non-flip) amplitude is non-zero in the forward limit and scales for $Q \rightarrow \infty$ as

$$\mathcal{A}_2^{1,1} \sim Q m_M \int dr r^2 K_1\left(\sqrt{z\bar{z}Q^2 r^2}\right) \sim \frac{1}{Q} \frac{m_M}{Q}. \quad (3.12)$$

The s -channel non-conserving helicity amplitudes are zero in the forward limit. For the longitudinal (transverse)-photon-to-transverse (longitudinal)-meson amplitude, $\mathcal{A}_2^{0,1}$ ($\mathcal{A}_2^{1,0}$), if we set $|\Delta| = 0$ in the phase factor in eq. (3.1), then the integral over z vanishes due to the anti-symmetric (symmetric) property of the $\varphi_1^T(z)$ ($\varphi_{\parallel}(z)$) under the exchange $z \rightarrow 1 - z$. The first leading contribution in the next-to-forward kinematics comes from the expansion at the first order in $|\Delta|$ of the phase factor and leads to the scaling behavior

$$\mathcal{A}_2^{0,1} \sim Q |\Delta| \int dr r^2 K_1 \left(\sqrt{z\bar{z}Q^2 r^2} \right) \sim \frac{1}{Q} \frac{|\Delta|}{Q}, \quad (3.13)$$

$$\mathcal{A}_2^{1,0} \sim Q m_M |\Delta| \int dr r^3 K_0 \left(\sqrt{z\bar{z}Q^2 r^2} \right) \sim \frac{1}{Q} \frac{m_M}{Q} \frac{|\Delta|}{Q}, \quad (3.14)$$

in the $Q \rightarrow \infty$ limit. The transverse-photon-to-transverse-meson s -channel helicity-non-conserving (flip) amplitude is particularly interesting, because it is zero in the forward and next-to-forward limits. Indeed, in this case, the vanishing is due to the angular integrals

$$\int_0^{2\pi} d\varphi e^{\pm i2\varphi} = 0 \quad \text{and} \quad \int_0^{2\pi} d\varphi \cos \varphi e^{\pm i2\varphi} = 0, \quad (3.15)$$

appearing at forward and next-to-forward accuracy, respectively. If one goes beyond that in the perturbative part of the amplitude, the scaling reads

$$\mathcal{A}_2^{-1,1} \sim Q m_M |\Delta|^2 \int dr r^4 K_1 \left(\sqrt{z\bar{z}Q^2 r^2} \right) \sim \frac{1}{Q} \frac{m_M}{Q} \frac{|\Delta|^2}{Q^2}. \quad (3.16)$$

Thus, if $m_M \gg |\Delta|$, one find the hierarchy $\mathcal{A}_2^{0,0} > \mathcal{A}_2^{1,1} > \mathcal{A}_2^{0,1} > \mathcal{A}_2^{1,0}, \mathcal{A}_2^{-1,1}$, experimentally observed at HERA [82].

3.2 Helicity amplitudes: 3-body Fock state

At twist-3 accuracy, the amplitude receives contributions from the three-body Fock state, which includes the quark, the antiquark, and an additional gluon. The most general structure of this contribution can be written in terms of the overlap between the photon/meson wavefunctions and Wilson line correlators involving up to four Wilson lines. This expression involves an integration over the longitudinal momentum fractions of the constituents, constrained by momentum conservation, as well as over their transverse positions. In Ref. [117], it was found to be

$$\begin{aligned} \mathcal{A}_3 = & \left(\prod_{i=1}^3 \int dx_i \theta(x_i) \right) \delta \left(1 - \sum_i x_i \right) \int d^2 z_1 d^2 z_2 d^2 z_3 e^{i\mathbf{q}(x_1 \mathbf{z}_1 + x_2 \mathbf{z}_2 + x_3 \mathbf{z}_3)} \\ & \times \Psi_3(\{x\}, \{z\}) \left\langle P(p') \left| \mathcal{U}_{z_1 z_3} \mathcal{U}_{z_3 z_2} - \mathcal{U}_{z_1 z_3} - \mathcal{U}_{z_3 z_2} + \frac{1}{N_c^2} \mathcal{U}_{z_1 z_2} \right| P(p) \right\rangle, \end{aligned} \quad (3.17)$$

where the photon/meson wavefunction overlap reads

$$\Psi_3(\{x\}, \{z\}) = \frac{e_q m_M}{8\pi} \left(\varepsilon_{q\rho} - \frac{\varepsilon_q^+}{q^+} q_\rho \right) \left(\varepsilon_M^{*\mu} - \frac{p_M^\mu}{p_M^+} \varepsilon_M^{*+} \right) \delta \left(1 - \frac{p_M^+}{q^+} \right) \left(\prod_{j=1}^3 \theta(x_j) \theta(1 - x_j) e^{-i x_j \mathbf{p}_M \mathbf{z}_j} \right)$$

$$\begin{aligned}
& \times c_f \left\{ f_{3M}^V g_{\sigma\mu} V(x_1, x_2) \left[\left(4g_{\perp}^{\rho\sigma} \frac{x_1 x_2}{1-x_2} \frac{Q}{Z} K_1(QZ) - iT_1^{\sigma\rho\nu}(\{x\}) \frac{z_{23\perp\nu}}{z_{23}^2} K_0(QZ) \right) - (1 \leftrightarrow 2) \right] \right. \\
& \left. - \epsilon_{-\sigma\beta} f_{3M}^A g_{\perp\mu}^{\beta} A(x_1, x_2) \left[\left(4\epsilon^{\sigma\rho+-} \frac{x_1 x_2}{1-x_2} \frac{Q}{Z} K_1(QZ) + T_2^{\sigma\rho\nu}(\{x\}) \frac{z_{23\perp\nu}}{z_{23}^2} K_0(QZ) \right) + (1 \leftrightarrow 2) \right] \right\}, \tag{3.18}
\end{aligned}$$

with

$$\begin{aligned}
& T_1^{\sigma\rho\nu}(\{x\}) \\
& = 4 \left[2x_1 q^{\rho} \left(2\frac{x_2}{x_3} + 1 \right) g_{\perp}^{\sigma\nu} - \left(2\frac{x_1-x_2}{x_3} g_{\perp}^{\sigma\nu} g_{\perp}^{\rho\mu} - \frac{g_{\perp}^{\alpha\nu} g_{\perp}^{\rho\sigma} + g_{\perp}^{\sigma\nu} g_{\perp}^{\rho\alpha} - g_{\perp}^{\alpha\sigma} g_{\perp}^{\rho\nu}}{x_2+x_3} \right) i\partial_{z_{1\perp\alpha}} \right] \\
& \equiv 4 \left[2x_1 q^{\rho} \left(2\frac{x_2}{x_3} + 1 \right) g_{\perp}^{\sigma\nu} - \Xi_1^{\alpha\nu\rho\sigma} i\partial_{z_{1\perp\alpha}} \right],
\end{aligned}$$

$$\begin{aligned}
& T_2^{\sigma\rho\nu}(\{x\}) \\
& = \frac{4i}{\bar{x}_1} \left[2x_1 \bar{x}_1 q^{\rho} \epsilon^{\nu\sigma+-} - \left(\left(1 + \frac{2x_2}{x_3} \right) (g_{\perp}^{\sigma\alpha} \epsilon^{\nu\rho+-} - g_{\perp}^{\rho\sigma} \epsilon^{\nu\alpha+-}) + (x_1 - \bar{x}_1) g_{\perp}^{\rho\alpha} \epsilon^{\nu\sigma+-} \right) i\partial_{z_{1\perp\alpha}} \right] \\
& \equiv \frac{4i}{\bar{x}_1} \left[2x_1 \bar{x}_1 q^{\rho} \epsilon^{\nu\sigma+-} - \Xi_2^{\alpha\nu\rho\sigma} i\partial_{z_{1\perp\alpha}} \right],
\end{aligned}$$

and

$$c_f = \frac{N_c^2}{N_c^2 - 1}, \quad Z = \sqrt{x_1 x_2 z_{12}^2 + x_1 x_3 z_{13}^2 + x_2 x x z_{23}^2}. \tag{3.19}$$

The $(1 \leftrightarrow 2)$ transformation means $(x_1, \mathbf{z}_1 \leftrightarrow x_2, \mathbf{z}_2)$ and should not be confused with the $(x_1 \leftrightarrow x_2)$ transformation.

The completely general expression given above can be strongly simplified in the pure dipole limit, i.e. neglecting the product of two dipole operators in eq. (3.17)³. In this limit, the 6-dimensional integration over the transverse coordinates can be reduced to a 2-dimensional integral, significantly easing numerical evaluations. Furthermore, in models with radial symmetry, such as the McLerran–Venugopalan model, angular integrations become trivial. The detailed derivation of these simplifications is provided in Appendix C, where both the main steps and the required integrals are worked out.

In the numerical analysis of the present work, we will consider only the $T \rightarrow T$ transition, which is the only one surviving in the forward limit. However, by performing a non-trivial expansion around $\Delta = 0$ (i.e. relaxing the strictly forward direction), we will also extract, for the first time, the dominant contribution of the longitudinal-photon-to-transverse-meson amplitudes in the quasi-forward limit.

To streamline the notation in the results that follow, we define effective mass parameters associated with the longitudinal momentum fractions,

$$\mu_i = \sqrt{x_i \bar{x}_i} Q^2, \quad \mu_{ij} = \sqrt{\frac{x_i x_j}{x_i + x_j}} Q^2, \tag{3.20}$$

³Please note that this does not mean neglecting non-linear saturation effects due to the evolution, which are incorporated through the evolution of the dipole.

as well as the dimensionless ratios of the twist-3 decay constants to the leading-twist one,

$$\zeta_{3M}^A = \frac{f_{3M}^A}{f_M}, \quad \zeta_{3M}^V = \frac{f_{3M}^V}{f_M}. \quad (3.21)$$

Moreover, we define the overall prefactors

$$\begin{aligned} \mathcal{C}_L &= -(2\pi)^4 \delta^{(4)}(q + p_t - p_M - p_{t'}) W^2 e_q m_M f_M, \\ \mathcal{C}_T &= -2(2\pi)^4 \delta^{(4)}(q + p_t - p_M - p_{t'}) W^2 \frac{e_q m_M f_M}{Q^2}. \end{aligned} \quad (3.22)$$

encoding the normalization of the longitudinal and transverse amplitudes, respectively.

Longitudinal-photon-to-transverse-meson amplitude. Starting from eq. (C.36) and replacing the explicit expression of the $F_i(x_i, x_j, \mathbf{r}^2)$ and $\tilde{F}_i(x_i, x_j, \mathbf{r}^2)$ functions in the appendix C.4, for the longitudinal-to-transverse helicity transition, we obtain

$$\begin{aligned} \mathcal{A}_3^{T,L} &= \mathcal{C}_L \int \frac{d^2\mathbf{r}}{2\pi} \mathcal{U}(\mathbf{r}) \left[(\boldsymbol{\varepsilon}_M^* \cdot \boldsymbol{\Delta}) \frac{\varepsilon_q^+}{q^+} \right] \left[\prod_{i=1}^3 \int dx_i \right] \delta \left(1 - \sum_i x_i \right) \\ &\quad \times \left(\zeta_{3M}^A A(x_1, x_2) - \left(1 + \frac{2x_2}{x_3} \right) \zeta_{3M}^V V(x_1, x_2) \right) \\ &\quad \times \left\{ \left(\frac{N_c}{C_F} - 2 \right) \left[-\frac{x_1}{x_3} \mu_1 |\mathbf{r}| K_1(\mu_1 |\mathbf{r}|) + \frac{x_1}{x_3(x_1 + x_2)} \mu_{12} |\mathbf{r}| K_1(\mu_{12} |\mathbf{r}|) \right] \right. \\ &\quad \left. + \frac{N_c}{C_F} \left[-\frac{x_1}{x_2} \mu_1 |\mathbf{r}| K_1(\mu_1 |\mathbf{r}|) + \frac{x_1}{x_2(x_1 + x_3)} \mu_{13} |\mathbf{r}| K_1(\mu_{13} |\mathbf{r}|) + \frac{x_2}{(x_2 + x_3)^2} \mu_{23} |\mathbf{r}| K_1(\mu_{23} |\mathbf{r}|) \right] \right\}. \end{aligned} \quad (3.23)$$

Transverse-photon-to-transverse-meson-transition amplitudes. Similarly, the helicity non-flip part of the transverse-to-transverse helicity amplitude reads

$$\begin{aligned} \mathcal{A}_{3,\text{n.f.}}^{T,T} &= \mathcal{C}_T \int \frac{d^2\mathbf{r}}{2\pi} \mathcal{U}(\mathbf{r}) \frac{T_{\text{n.f.}}}{2} \left[\prod_{i=1}^3 \int_0^1 dx_i \right] \frac{\delta(1 - \sum_i x_i)}{x_1} \left(\frac{\zeta_{3M}^A A(x_1, x_2) + \zeta_{3M}^V V(x_1, x_2)}{x_3} \right) \\ &\quad \times \left\{ \left(\frac{N_c}{C_F} - 2 \right) \left[\frac{1}{x_3} \mu_1^2 K_0(\mu_1 |\mathbf{r}|) + \frac{\bar{x}_2}{x_2 x_3} \mu_2^2 K_0(\mu_2 |\mathbf{r}|) - \frac{1}{x_3} \left(1 + \frac{\bar{x}_2}{x_2} \right) \mu_{12}^2 K_0(\mu_{12} |\mathbf{r}|) \right] \right. \\ &\quad \left. + \frac{N_c}{C_F} \left[\frac{\bar{x}_2}{x_1 x_2} \mu_2^2 K_0(\mu_2 |\mathbf{r}|) + \frac{1}{\bar{x}_1} \left(1 - \frac{\bar{x}_1 \bar{x}_2}{x_1 x_2} \right) \mu_{23}^2 K_0(\mu_{23} |\mathbf{r}|) + \frac{2}{\bar{x}_1} \mu_1^2 K_0(\mu_1 |\mathbf{r}|) \right] \right\}, \end{aligned} \quad (3.24)$$

while the helicity flip part is

$$\begin{aligned} \mathcal{A}_{3,\text{f.}}^{T,T} &= \mathcal{C}_T \int \frac{d^2\mathbf{r}}{2\pi} \mathcal{U}(\mathbf{r}) T_{\text{f.}}(\mathbf{r}) \left[\prod_{i=1}^3 \int_0^1 dx_i \right] \frac{\delta(1 - \sum_i x_i)}{x_1} \left(\frac{\zeta_{3M}^A A(x_1, x_2) + \zeta_{3M}^V V(x_1, x_2)}{x_3} \right) \\ &\quad \times \left\{ \frac{N_c}{C_F} \left[\mu_{qg}^2 K_2(\mu_{qg} |\mathbf{r}|) + \mu_{\bar{q}g}^2 K_2(\mu_{\bar{q}g} |\mathbf{r}|) - \mu_1^2 K_2(\mu_1 |\mathbf{r}|) - \mu_2^2 K_2(\mu_2 |\mathbf{r}|) \right] + \left(\frac{N_c}{C_F} - 2 \right) \right. \\ &\quad \left. \times \left[\frac{x_2}{x_3} \left(\mu_{q\bar{q}}^2 K_2(\mu_{q\bar{q}} |\mathbf{r}|) - \mu_1^2 K_2(\mu_1 |\mathbf{r}|) \right) + \frac{x_1}{x_3} \left(\mu_{q\bar{q}}^2 K_2(\mu_{q\bar{q}} |\mathbf{r}|) - \mu_2^2 K_2(\mu_2 |\mathbf{r}|) \right) \right] \right\}. \end{aligned} \quad (3.25)$$

4 Numerical results

In this section, we first compare our framework with HERA measurements of exclusive vector meson electroproduction, focusing on two helicity-sensitive observables. We then turn to predictions for the future Electron–Ion Collider (EIC), where scattering off a heavy nuclear target (we consider lead) is expected to enhance saturation effects compared to the proton case.

We consider two observables that were extensively studied at HERA in exclusive vector meson production [82]. The first one is the helicity-conserving transverse-to-longitudinal amplitude ratio

$$R_{11} = \frac{\mathcal{A}^{11}}{\mathcal{A}^{00}}, \quad (4.1)$$

This ratio provides direct information on the relative importance of transverse and longitudinal photon polarizations. The second observable is the spin-density matrix element r_{00}^{04} , which can be expressed in terms of helicity amplitudes as

$$r_{00}^{04} = \frac{\varepsilon + R_{01}^2}{R_{11}^2 + \varepsilon + R_{01}^2 + R_{1-1}^2 + 2\varepsilon R_{10}^2}, \quad (4.2)$$

where ε denotes the virtual photon polarization parameter and $R_{\lambda_V \lambda_\gamma} \equiv \mathcal{A}^{\lambda_V \lambda_\gamma} / \mathcal{A}^{00}$ are ratios of helicity amplitudes normalized to the longitudinal one.

In the limit of small momentum transfer ($t \rightarrow 0$), where helicity is approximately conserved (s-channel helicity conservation, SCHC), the helicity-flip amplitudes are suppressed, i.e. $R_{10}, R_{01}, R_{1-1} \ll 1$. Under this assumption, the expression simplifies to

$$r_{00}^{04} \simeq \frac{\varepsilon}{R_{11}^2 + \varepsilon}. \quad (4.3)$$

In the present analysis, we adopt this approximation, which is justified in the near-forward kinematics. However, it is important to stress that, beyond the strict SCHC limit, a direct comparison between r_{00}^{04} and R_{11} is non-trivial. While R_{11} is defined purely in terms of helicity-conserving amplitudes, the experimental extraction of r_{00}^{04} receives contributions from helicity-flip transitions and from non-zero momentum transfer. As a consequence, the one-to-one correspondence implied by the above relation is not exact at the experimental level, and the two observables should be regarded as complementary rather than redundant probes of the underlying dynamics.

For H1, one has $\langle \varepsilon \rangle = 0.98$, while for ZEUS $\langle \varepsilon \rangle = 0.996$, indicating an almost purely longitudinal photon flux. For the EIC, we will assume $\langle \varepsilon \rangle = 1$, which is an excellent approximation in the high-energy limit.

4.1 Helicity amplitudes ratio and spin-density matrix element r_{00}^{04} at the HERA and the EIC

In Fig. 1, we compare our results with the data of the H1 experiment [82] at HERA at fixed $W = 100$ GeV. We study both linear (BFKL) and non-linear (BK) small- x evolution.

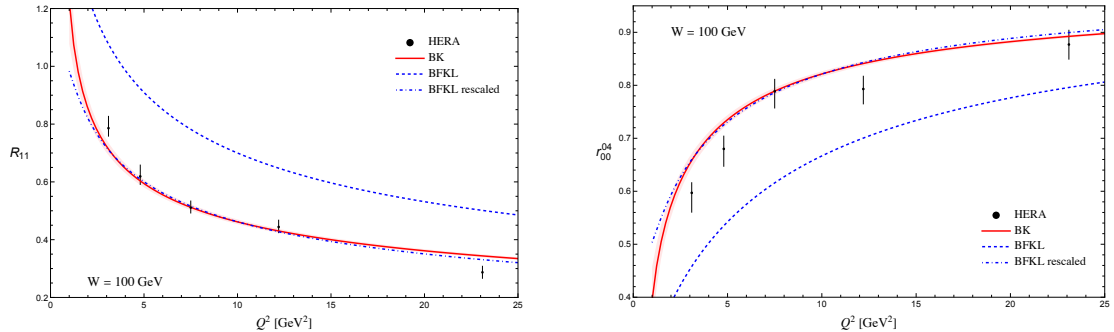


Figure 1. Predictions for the helicity-amplitude ratio R_{11} (left) and for the spin-density matrix element r_{00}^{04} (right), as a function of Q^2 at fixed $W = 100$ GeV, are compared to the data of H1 [82]. The red curves denote predictions obtained by evolving the initial condition in eq. (2.16) through the non-linear BK evolution. The dashed and dashed-dot blue lines are both obtained by evolving the initial condition in eq. (2.16) through the linear BFKL evolution; the dashed-dot one is rescaled by a constant factor in order to match the BK prediction at high Q^2 . The error bands around the non-linear prediction show only the uncertainty due to the non-perturbative parameters of the DAs.

The parameters entering the initial conditions were originally fitted on DIS data [124], considering the BK evolution only. Therefore, in order to perform a meaningful comparison with the purely linear BFKL evolution, we readjust the overall normalization of the BFKL solution. The rescaling is fixed by imposing that, at sufficiently large Q^2 , the BFKL and BK predictions coincide. This choice is physically motivated by the fact that saturation effects are expected to be relevant predominantly at low and moderate Q^2 , while at large Q^2 the dynamics should be governed by linear evolution. In this way, we emphasize the difference in shape observed at low Q^2 , which can be attributed to non-linear (saturation) effects. It is, however, important to note that the rescaling procedure applied to BFKL, while very reasonable, is not optimal—namely, it does not exactly correspond to a fit to DIS data performed with the present initial conditions and with non-linear effects switched off. We will return to this point in the following.

As shown in Fig. 1, the BK evolution leads to a modification of both R_{11} and r_{00}^{04} in the low- Q^2 region, while the two approaches converge at large Q^2 , consistently with expectations. This suggests that helicity amplitude ratios and spin-density matrix elements are sensitive to saturation dynamics in exclusive processes. The observables under consideration are ratios of helicity amplitudes and related spin-density matrix elements. Being ratios, they are not a priori guaranteed to exhibit a sensitivity to saturation dynamics, since part of the underlying gluon-density dependence may cancel. For this reason, it is non-trivial to assess that the non-linear (saturation) effects leave a visible imprint in the low- Q^2 region, where they are expected to be most relevant. Quantitatively, the linear and nonlinear predictions begin to separate around 3 GeV^2 , reaching a 6 % difference at 2 GeV^2 . A significant difference (20 %) is observed only around 1 GeV^2 , which is similar to the saturation scale expected for a proton at this center-of-mass energy.

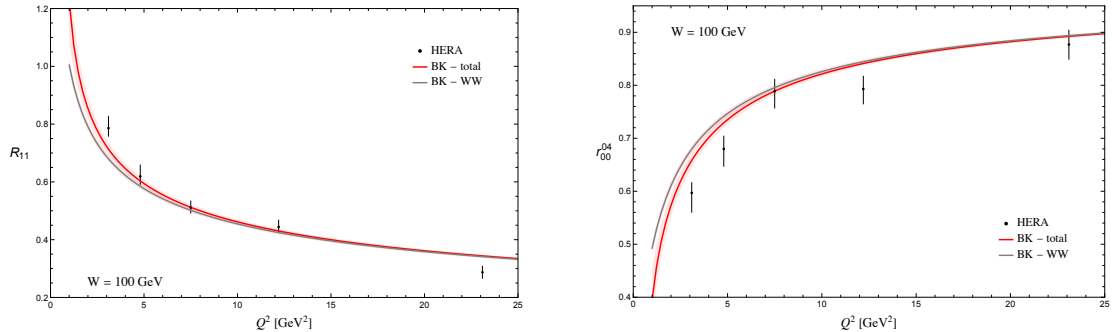


Figure 2. Predictions for the helicity amplitudes ratio R_{11} (left) and for the spin-density matrix element r_{00}^{04} (right), as a function of Q^2 at fixed $W = 100$ GeV, are compared to the data of H1 [82]. Both curves are obtained by evolving the initial condition in eq. (2.16) through the non-linear BK evolution. The error bands around the non-linear prediction show only the uncertainty due to the non-perturbative parameters of the DAs.

As noted above, the BFKL result has been rescaled by an overall factor in order to match the BK prediction at a sufficiently large value of Q^2 , where saturation effects are expected to be negligible. We have chosen $Q^2 = 10$ GeV², which is roughly an order of magnitude larger than the typical saturation scale for a proton in HERA kinematics. However, as is evident from Figs. 1 and 3, the two predictions are slightly misaligned, such that a simple normalization at a fixed Q^2 cannot ensure agreement over the entire high- Q^2 region. That said, the comparison between BK and BFKL is only non-trivial at low Q^2 , where this mismatch leads at most to an effect of a few percent, which is negligible at the level of accuracy considered here⁴. In any case, the small discrepancies observed at high Q^2 (or moderate W^2) between BFKL and BK in our plots should not be interpreted as physical, but rather as an artifact of this normalization procedure.

As is well known, at the energies accessible at present colliders the saturation scale lies in the perturbative domain. This opens the possibility of investigating the nonlinear regime of QCD using the perturbative tools of the semi-classical small- x effective theory. However, with the exception of fully inclusive processes—most notably DIS—phenomenologically relevant observables sensitive to gluon saturation are typically described within the so-called hybrid factorization framework. In this approach, non-perturbative inputs encoding the partonic structure of hadrons or the hadronization of the final state (*e.g.*, fragmentation functions or distribution amplitudes) are introduced. In doing so, genuine higher-twist contributions—such as the three-body component of the DAs considered in this work—are systematically neglected. At most, kinematic twist corrections are included, retaining the transverse-momentum dependence of the lowest Fock states.

Nevertheless, although saturation effects enter a perturbative regime at current collider energies, the value of the saturation scale is not sufficiently large to suppress *a priori* genuine higher-twist contributions (*i.e.* higher Fock components). Since our calculation

⁴In particular, in the absence of NLO corrections to the impact factors.

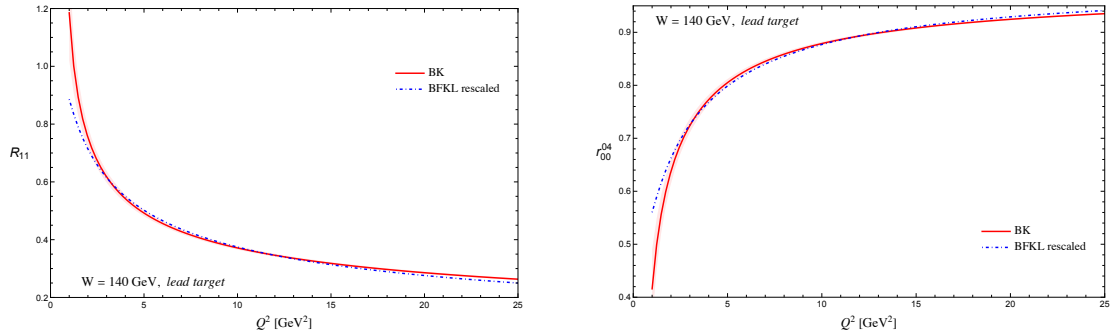


Figure 3. Predictions for the helicity amplitudes ratio R_{11} (left) and for the spin-density matrix element r_{00}^{04} (right), as a function of Q^2 at fixed $W = 140$ GeV. The red curves denote the predictions obtained by evolving the initial condition in eq. (2.16) through the non-linear BK evolution. The dashed-dot blue line is obtained by evolving the initial condition in eq. (2.16) through the linear BFKL evolution and by rescaling a constant factor to match the BK prediction at high Q^2 . The error bands around the non-linear prediction show only the uncertainty due to the non-perturbative parameters of the DAs.

consistently incorporates both genuine and kinematic twist-3 terms, it allows us to assess their relative importance at low Q^2 . Figure 2 illustrates the impact of removing the genuine twist-3 contribution: the effect on the helicity ratio and on the spin-density matrix element r_{04}^{00} is typically larger than that of saturation. It becomes visible below 10 GeV² and reaches 15 % already at 2 GeV², while it is the same size as non-linear evolution effects at 1 GeV². Although observables whose leading contribution arises at twist-2 are expected to be less sensitive to genuine higher-twist effects, these contributions are nevertheless not negligible in view of precise measurements of gluon saturation. For instance, from Fig. 2, one can estimate that the impact on the total cross section ranges from approximately 18 % down to about a few % in the interval $1 \text{ GeV}^2 \leq Q^2 \leq 5 \text{ GeV}^2$.

We now present predictions for DVMP at the EIC in electron–lead collisions. Figure 3 shows R_{11} and r_{00}^{04} for a lead target as functions of Q^2 at fixed $W = 140$ GeV. As expected, saturation effects are more pronounced for the lead target, although the increase is relatively modest. At $Q^2 = 1$ GeV², the magnitude of the saturation effects is approximately 25% in Fig. 3, whereas in Fig. 1 it was about 20%. Figure 4 shows the trend in energy at fixed values of Q^2 . The flat behavior of the ratios is consistent with what was previously observed at HERA (see Fig. 39 in Ref. [82]). As shown in both plots, the linear and nonlinear predictions differ at small values of Q^2 . However, this difference gradually diminishes and becomes negligible as Q^2 increases. This difference remains nearly constant across the explored energy range.

5 Conclusions and Outlook

In this work, we have extended our previous analysis of Deeply Virtual Meson Production, performing a detailed phenomenological study within the Color Glass Condensate framework. We have investigated two helicity-sensitive observables, the transverse-to-longitudinal

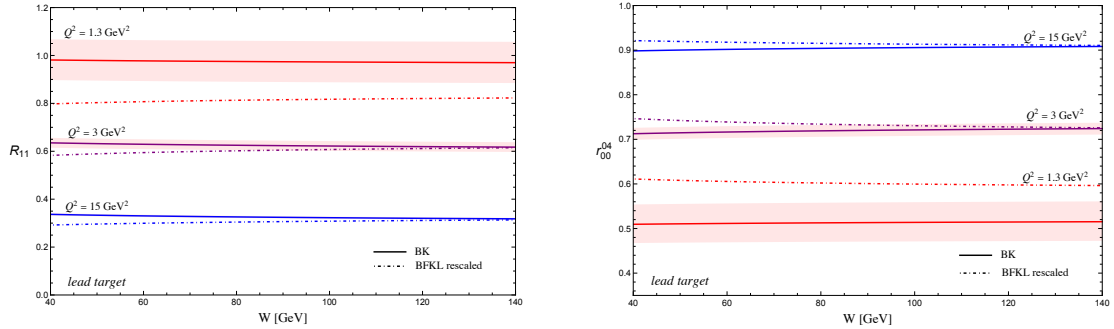


Figure 4. Predictions for the helicity amplitudes ratio R_{11} (left) and for the spin-density matrix element r_{00}^{04} (right), as a function of W for different values of Q^2 : 1.3 GeV^2 , 3 GeV^2 and 15 GeV^2 . The red curves denote the predictions obtained by evolving the initial condition in eq. (2.16) through the non-linear BK evolution. The dashed-dot blue line is obtained by evolving the initial condition in eq. (2.16) through the linear BFKL evolution and by rescaling a constant factor to match the BK prediction at high Q^2 . The error bands around the non-linear prediction show only the uncertainty due to the non-perturbative parameters of the DAs.

amplitude ratio $R_{11} = \mathcal{A}^{11}/\mathcal{A}^{00}$ and the spin-density matrix element r_{00}^{04} , including small- x evolution through numerical solutions of the running-coupling and collinearly improved BK and BFKL equations with the McLerran–Venugopalan model as initial condition.

The obtained predictions (shown on the Figs. 1, 3, and 4) based on BK and BFKL evolutions match at large Q^2 , with differences emerging at low Q^2 . Comparing our results with the HERA data, we observed that the low- Q^2 trends of the observables suggest a slightly improved agreement with a nonlinear small- x evolution, offering encouraging hints of possible signals of the onset of gluon saturation. Although the considered observables are ratios of helicity amplitudes—where part of the gluon-density dependence may cancel—we observe that they retain a non-trivial sensitivity to non-linear dynamics.

Furthermore, thanks to the consistent inclusion of both kinematic and genuine twist-3 contributions, we have quantified the role of higher Fock-state components of the light vector meson distribution amplitudes. We have demonstrated that genuine higher-twist effects are sizable in the kinematic region relevant for saturation physics at forthcoming experiments. This highlights the importance of a systematic treatment of higher-twist contributions in exclusive processes probing the small- x regime.

We have also provided predictions for electron–lead collisions at the future Electron–Ion Collider, shown on the Figs. 3 and 4. Saturation effects are enhanced for a heavy nuclear target, leading to a slightly more pronounced separation between linear and non-linear evolution scenarios at low Q^2 , while the two approaches converge at larger virtualities.

From the theoretical side, a natural and compelling step is to extend the present analysis to full next-to-leading logarithmic accuracy by including the currently unknown NLO

corrections to the impact factors⁵, which we plan to compute in the near future. Including also this class of NLO corrections is particularly important to corroborate our observations on the low- Q^2 trend⁶.

An important phenomenological development will be the investigation of the full set of spin-density matrix elements in ρ -meson production, obtained in [80, 117]. A comprehensive analysis of these observables will provide additional tests of small- x and saturation dynamics and of the interplay between non-linear evolution and higher-twist effects in exclusive processes at the EIC.

Acknowledgments

We thank Guillaume Beuf, Piotr Korcyl, and Leszek Motyka for useful discussions. The work of L.D.R. and A.P. is supported by the INFN/QFT@COLLIDERS project (Italy) and by the European Union – Next Generation EU through the research grant number P2022Z4P4B “SOPHYA - Sustainable Optimised PHYSics Algorithms: fundamental physics to build an advanced society” under the program PRIN 2022 PNRR of the Italian Ministero dell’Università e Ricerca. The work of L.D.R. has also been supported by the research grant number 20227S3M3B “Bubble Dynamics in Cosmological Phase Transitions” under the program PRIN 2022 of the Italian Ministero dell’Università e Ricerca. The work of M.F. is supported by the ULAM fellowship program of NAWA No. BNI/ULM/2024/1/00065 “Color glass condensate effective theory beyond the eikonal approximation”. L. S. was supported by the Grant No. 2024/53/B/ST2/00968 of the National Science Center in Poland.

A.P., L.D.R., L.S. and M.F. gratefully acknowledge the warm hospitality and financial support of IJCLab, where part of this work was carried out. This work was supported by the "P2I - Graduate School of Physics", in the framework “Investissements d’Avenir” (ANR-11-IDEX-0003-01) managed by the Agence Nationale de la Recherche (ANR), France. This work was also supported in part by the European Union’s Horizon 2020 research and innovation program under Grant Agreement No. 824093 (Strong2020). This project has also received funding from the French Agence Nationale de la Recherche (ANR) via the grant ANR-20-CE31-0015 (“PrecisOnium”) and was also partly supported by the French CNRS via the COPIN-IN2P3 bilateral agreement and via the IN2P3 project “QCDFactorisation@NLO”.

A Evolutions of DAs as a function of μ

The parameters entering the DAs at $\mu = 1$ GeV and their evolution equations are given in Ref. [125]. In Table 1 we recall their values for the ρ meson at $\mu_0 = 1$ GeV.

⁵The NLO corrections are known only for the longitudinal-to-longitudinal transition [60, 61, 127], which is not enough to provide a description of the present observables at NLO.

⁶Although our analysis contains the logarithmically enhanced NLO terms (running coupling and collinear effects), for $Q^2 \sim$ a few GeV², terms of the order of α_s/π are expected to be sizable and necessary for definitive statements on the present observables.

α_s	0.52
$\omega_{\{1,0\}}^A$	-2.1
$\omega_{[0,1]}^V$	28/3
$a_{2,\rho}$	0.18 ± 0.10
$m_\rho f_{3\rho}^A$	$0.5\text{-}0.6 \cdot 10^{-2} \text{ GeV}^2$
$m_\rho f_{3\rho}^V$	$0.2 \cdot 10^{-2} \text{ GeV}^2$
$f_{3\rho}^A/f_\rho$	0.032
$f_{3\rho}^V/f_\rho$	0.013

Table 1. Coupling constants and Gegenbauer coefficients entering the ρ -meson DAs, at the scale $\mu_0 = 1 \text{ GeV}$. Please note that in Ref. [125] the normalization is such that $f_{3\rho}^{V,A}[\text{125}] = m_\rho f_{3\rho}^{V,A}[\text{here}]$ and $\omega_{[0,1]}^V$ and f_ρ are fixed constant.

For a_2 , the evolution equation is

$$a_2(\mu^2) = a_2(\mu_0^2) L(\mu^2)^{\gamma_2/b_0}, \quad (\text{A.1})$$

with

$$L(\mu^2) = \frac{\alpha_s(\mu^2)}{\alpha_s(\mu_0^2)} = \frac{1}{1 + \frac{b_0}{\pi} \alpha_s(\mu_0^2) \ln(\mu^2/\mu_0^2)}, \quad (\text{A.2})$$

where $b_0 = (11N_c - 2N_f)/3$, $\gamma_n = 4C_F \left(\psi(n+2) + \gamma_E - \frac{3}{4} - \frac{1}{2(n+1)(n+2)} \right)$ and $\psi(n) = -\gamma_E + \sum_{k=1}^{n+1} 1/k$. For the $f_{3\rho}^A$ coupling constant, the evolution is given by

$$f_{3\rho}^A(\mu^2) = f_{3\rho}^A(\mu_0^2) L(\mu^2)^{\Gamma_2^-/b_0}, \quad (\text{A.3})$$

with $\Gamma_2^- = -\frac{C_F}{3} + 3C_g$ ($C_g = N_c$). The couplings $f_{3\rho}^V(\mu^2)$ and $\omega_{\{0,1\}}^A(\mu^2) f_{3\rho}^A(\mu^2)$ enter a matrix evolution equation [125]. Defining

$$V(\mu^2) = \begin{pmatrix} \omega_{[0,1]}^V f_{3\rho}^V(\mu^2) - \omega_{\{0,1\}}^A(\mu^2) f_{3\rho}^A(\mu^2) \\ \omega_{[0,1]}^V f_{3\rho}^V(\mu^2) + \omega_{\{0,1\}}^A(\mu^2) f_{3\rho}^A(\mu^2) \end{pmatrix}, \quad (\text{A.4})$$

it reads

$$V(\mu^2) = L(\mu^2)^{\Gamma_3^+/b_0} V(1), \quad (\text{A.5})$$

with Γ_3^+ given by

$$\Gamma_3^+ = \begin{pmatrix} \frac{8}{3}C_F + \frac{7}{3}C_g & \frac{2}{3}C_F - \frac{2}{3}C_g \\ \frac{5}{3}C_F - \frac{4}{3}C_g & \frac{1}{6}C_F + 4C_g \end{pmatrix}. \quad (\text{A.6})$$

Hence, by diagonalizing the system, we can determine the scale dependence of $f_{3\rho}^V(\mu^2)$ and $\omega_{\{0,1\}}^A(\mu^2)$, thereby obtaining the running of all four coupling constants.

B Explicit parametrization of the set of DAs

The independent DAs are given in eqs. (2.18), (2.19), and (2.20), we report them here for convenience of the reader⁷

$$\begin{aligned}\varphi_{\parallel}(z) &= 6z(1-z) \left(1 + \frac{3}{2}a_2(\mu^2)(5(2z-1)^2-1) \right), \\ V(x_1, x_2) &= 5040 x_1 x_2 (x_1 - x_2)(1 - x_1 - x_2)^2, \\ A(x_1, x_2) &= 360 x_1 x_2 \left(1 + \frac{\omega_{\{1,0\}}^A(\mu^2)}{2}(4 - 7(x_1 + x_2)) \right) (1 - x_1 - x_2)^2.\end{aligned}$$

The result in Ref. [117] is expressed in terms of DAs that can be explicitly constructed from these three; this is the scope of the present appendix.

Vector DAs. For the vector part, in Ref. [117], the 2-body twist-3 corrections are expressed in terms of the combination of DAs: $\tilde{h}(z) - h(z)$, which naturally emerge in the context of the Covariant Collinear Factorization (CCF) [125]. To build an explicit parametrization, we can exploit the relation to the set of DAs derived in the context of Light-Cone Collinear Factorization (LCCF) [104]⁸

$$\tilde{h}(z) - h(z) = \varphi_1^T(z) \equiv \varphi_1^T(z)|_{\text{W.W.}} + \varphi_1^T(z)|_{\text{G.T.}}, \quad (\text{B.1})$$

where (see eq. (88) in Ref. [104])

$$\begin{aligned}\varphi_1^T(z)|_{\text{W.W.}} &= \frac{1}{2} \left[-\bar{z} \int_0^z du \frac{\varphi_{\parallel}(u)}{\bar{u}} + z \int_z^1 du \frac{\varphi_{\parallel}(u)}{u} \right] \\ &= \frac{3}{2}z(2z^2 - 3z + 1) \left(1 + a_2(\mu^2)(1 + 15z(z-1)) \right),\end{aligned} \quad (\text{B.2})$$

and (see eq. (97) in Ref. [104] and eq. (B.5) here)

$$\begin{aligned}\varphi_1^T(z)|_{\text{G.T.}} &= \int_0^z dy \varphi_3^{\text{gen}}(y) \\ + \zeta_{3M}^V \int_0^z dx_1 \int_0^{1-x_1} dx_2 \frac{V(x_1, x_2)}{(1-x_1-x_2)^2} &= \int_0^z dy \varphi_3^{\text{gen}}(y) + 840\zeta_{3M}^V z^2(1-z)^2(2z-1),\end{aligned} \quad (\text{B.3})$$

where (see eq. (96) in Ref. [104])

$$\varphi_3^{\text{gen}}(y) = -\frac{1}{2} \int_y^1 \frac{du}{u} \left[\int_0^u dy_2 \frac{d}{du} (\zeta_{3M}^V B(y_2, u) - \zeta_{3M}^A D(y_2, u)) \right]$$

⁷We also employ the definitions in eq. (3.21).

⁸See eq. (B.29) in Ref. [117].

$$\begin{aligned}
& - \int_u^1 \frac{dy_2}{y_2 - u} (\zeta_{3M}^V B(u, y_2) - \zeta_{3M}^A D(u, y_2)) - \int_0^u \frac{dy_2}{y_2 - u} (\zeta_{3M}^V B(y_2, u) - \zeta_{3M}^A D(y_2, u)) \Big] \\
& \quad - \frac{1}{2} \int_0^y \frac{du}{\bar{u}} \left[\int_u^1 dy_2 \frac{d}{du} (\zeta_{3M}^V B(u, y_2) + \zeta_{3M}^A D(u, y_2)) \right. \\
& \left. - \int_u^1 \frac{dy_2}{y_2 - u} (\zeta_{3M}^V B(u, y_2) + \zeta_{3M}^A D(u, y_2)) - \int_0^u \frac{dy_2}{y_2 - u} (\zeta_{3M}^V B(y_2, u) + \zeta_{3M}^A D(y_2, u)) \right] ,
\end{aligned} \tag{B.4}$$

with

$$B(y_1, y_2) = -\frac{V(y_1, 1 - y_2)}{y_2 - y_1}, \quad D(y_1, y_2) = -\frac{A(y_1, 1 - y_2)}{y_2 - y_1}. \tag{B.5}$$

Performing the 2-dimensional integrations, we obtain

$$\begin{aligned}
\varphi_3^{\text{gen}}(y) = & -\frac{5}{8} \left(3\omega_{\{1,0\}}^A(\mu^2) (70y^4 - 140y^3 + 90y^2 - 20y + 1) \zeta_{3M}^A - 16 (6y^2 - 6y + 1) \zeta_{3M}^A \right. \\
& \left. - 84 (70y^4 - 140y^3 + 90y^2 - 20y + 1) \zeta_{3M}^V \right).
\end{aligned} \tag{B.6}$$

Then, for $\varphi_1^T(z)|_{\text{G.T.}}$, we have the parametrization

$$\begin{aligned}
\varphi_1^T(z)|_{\text{G.T.}} = & -\frac{5}{8} z (2z^2 - 3z + 1) \left[\zeta_{3M}^A \left(3\omega_{\{1,0\}}^A(\mu^2) (7z^2 - 7z + 1) - 16 \right) \right. \\
& \left. - 84 (23z^2 - 23z + 1) \zeta_{3M}^V \right].
\end{aligned} \tag{B.7}$$

Axial DAs. For the axial part, in Ref. [117], the 2-body twist-3 corrections are expressed in terms of the combination of DAs: $(-g_{\perp}^{(a)}(z) + \tilde{g}_{\perp}^{(a)}(z))/4$. Again, we can exploit the relation to the set of DAs derived in the context of Light-Cone Collinear Factorization (LCCF) [104]⁹

$$-\frac{g_{\perp}^{(a)}(z)}{4} + \frac{\tilde{g}_{\perp}^{(a)}(z)}{4} = \varphi_A^T(z) \equiv \varphi_A^T(z)|_{\text{w.w.}} + \varphi_A^T(z)|_{\text{G.T.}}, \tag{B.8}$$

where (see eq. (88) in Ref. [104])

$$\begin{aligned}
\varphi_A^T(z)|_{\text{w.w.}} = & -\frac{1}{2} \left[\bar{z} \int_0^z du \frac{\varphi_{\parallel}(u; \mu^2)}{\bar{u}} + z \int_z^1 du \frac{\varphi_{\parallel}(u; \mu^2)}{u} \right] \\
= & \frac{3}{2} z (z - 1) \left(1 + a_2(\mu^2) (1 + 5(z - 1)z) \right),
\end{aligned} \tag{B.9}$$

and (see eq. (99) in Ref. [104] and eq. (B.5) here)

$$\begin{aligned}
\varphi_A^T(z)|_{\text{G.T.}} = & \int_0^z dy \varphi_A^{\text{gen}}(y) + \zeta_{3M}^A \int_0^z dx_1 \int_0^{1-x_2} dx_2 \frac{A(x_1, x_2)}{(1 - x_1 - x_2)^2} \\
= & \int_0^z dy \varphi_A^{\text{gen}}(y) + 30 \zeta_{3M}^A \left(3 - \omega_{\{1,0\}}^A(\mu^2) \right) z^2 (1 - z)^2,
\end{aligned} \tag{B.10}$$

⁹See eq. (B.33) in Ref. [117].

where (see eq. (98) in Ref. [104])

$$\varphi_A^{\text{gen}}(y) = \varphi_3^{\text{gen}}(y) \Big|_{\zeta_{3M}^V B(x,y) \leftrightarrow \zeta_{3M}^A D(x,y)}. \quad (\text{B.11})$$

We can compute $\varphi_A^{\text{gen}}(y)$ explicitly and obtain

$$\varphi_A^{\text{gen}}(y) = -\frac{5}{8} (20y^3 - 30y^2 + 12y - 1) \left[\left(3\omega_{\{1,0\}}^A(\mu^2) - 16 \right) \zeta_{3M}^A - 84\zeta_{3M}^V \right]. \quad (\text{B.12})$$

Then, we get

$$\begin{aligned} \varphi_A^T(z) \Big|_{\text{G.T.}} &= \frac{5}{8} z(1-z) \left[\omega_{\{1,0\}}^A(\mu^2) (63z^2 - 63z + 3) \zeta_{3M}^A \right. \\ &\quad \left. - 16 (14z^2 - 14z + 1) \zeta_{3M}^A - 84 (5z^2 - 5z + 1) \zeta_{3M}^V \right]. \end{aligned} \quad (\text{B.13})$$

C Derivation of the dipole part of the 3-body amplitude

In the next subsections, we simplify the expressions obtained in Ref. [117], exploiting the quasi-forward limit. We will consider here only the dipole part of the amplitude.

C.1 $\mathcal{U}_{z_1 z_2}$ -part of the amplitude

We start by considering the $\mathcal{U}_{z_1 z_2}$ -part of the amplitude:

$$\begin{aligned} \mathcal{A}_3^{(a)} &= \left(\prod_{i=1}^3 \int_0^1 dx_i \right) \delta \left(1 - \sum_i x_i \right) \int d^2 z_1 d^2 z_2 e^{iq(x_1 z_1 + x_2 z_2)} \frac{\langle P(p') | \mathcal{U}_{z_1 z_2} | P(p) \rangle}{N_c^2} \\ &\quad \times \frac{e_q m_M}{8\pi} c_f \left(\varepsilon_{q\rho} - \frac{\varepsilon_q^+}{q^+} q_\rho \right) \left(\varepsilon_M^{*\mu} - \frac{p_M^\mu}{p_M^+} \varepsilon_M^{*+} \right) \delta \left(1 - \frac{p_M^+}{q^+} \right) \Psi_3^{(a)}(\{x\}, z_{12}), \end{aligned} \quad (\text{C.1})$$

where we defined the effective impact factor

$$\begin{aligned} \Psi_3^{(a)}(\{x\}, z_{12}) &= \int d^2 z_3 e^{ix_3(\mathbf{q}-\mathbf{p}_M)z_3} \left\{ f_{3M}^V g_{\sigma\mu} V(x_1, x_2) \left[\left(4g_\perp^{\rho\sigma} \frac{x_1 x_2}{1-x_2} \frac{Q}{Z} K_1(QZ) \right. \right. \right. \\ &\quad \left. \left. - 4i \left[2x_1 q^\rho \left(2\frac{x_2}{x_3} + 1 \right) g_1^{\sigma\nu} - \Xi_1^{\alpha\nu\rho\sigma} i\partial_{z_{1\perp}\alpha} \right] \frac{z_{23\perp\nu}}{z_{23}^2} K_0(QZ) \right) - (1 \leftrightarrow 2) \right] \\ &\quad - \epsilon_{-\sigma\beta} f_{3M}^A g_{\perp\mu}^\beta A(x_1, x_2) \left[\left(4\epsilon^{\sigma\rho+-} \frac{x_1 x_2}{1-x_2} \frac{Q}{Z} K_1(QZ) \right. \right. \\ &\quad \left. \left. + \frac{4i}{\bar{x}_1} \left[2x_1 \bar{x}_1 q^\rho \epsilon^{\nu\sigma+-} - \Xi_2^{\alpha\nu\rho\sigma} i\partial_{z_{1\perp}\alpha} \right] \frac{z_{23\perp\nu}}{z_{23}^2} K_0(QZ) \right) + (1 \leftrightarrow 2) \right] \right\}. \end{aligned} \quad (\text{C.2})$$

To perform the integration over z_3 we need the following integrals:

$$I_1^{(a)}(\{x\}, z_{12}) = \int d^2 z_3 e^{ix_3(\mathbf{q}-\mathbf{p}_M)z_3} \frac{Q}{Z} K_1(QZ), \quad (\text{C.3})$$

$$I_2^{(a)}(\{x\}, z_{12}) = \int d^2 z_3 e^{ix_3(\mathbf{q}-\mathbf{p}_M)z_3} \frac{z_{23\perp\nu}}{z_{23}^2} K_0(QZ), \quad (\text{C.4})$$

$$I_3^{(a)}(\{x\}, z_{12}) = \int d^2 z_3 e^{i x_3 (\mathbf{q} - \mathbf{p}_M) \cdot \mathbf{z}_3} \frac{z_{23\perp\nu}}{z_{23}^2} \frac{\partial}{\partial z_{1\perp}^\alpha} K_0(QZ) = \frac{\partial}{\partial z_{1\perp}^\alpha} I_2^{(a)}(\{x\}, z_{12}) . \quad (\text{C.5})$$

A couple of observations are in order. First, the symmetry under the exchange ($1 \leftrightarrow 2$) is preserved upon integration. Therefore, the contribution of the exchanged term can be obtained directly from the explicitly written expression in eq. (C.2). Our final goal is to integrate over \mathbf{z}_3 and then change variables to

$$\mathbf{r} = \mathbf{z}_1 - \mathbf{z}_2 , \quad \mathbf{b} = \frac{x_1 \mathbf{z}_1 + x_2 \mathbf{z}_2}{x_1 + x_2} , \quad (\text{C.6})$$

i.e. the dipole size and impact parameter characterizing the quark-antiquark dipole. When this is done, the dependence on \mathbf{b} results in a trivial exponential factor that can be integrated to obtain transverse momentum conservation, $\delta^{(2)}(\mathbf{q} - \mathbf{p}_M - \mathbf{\Delta})$. Since we are interested in near-to-forward kinematics when calculating the above-mentioned integrals, we can take this into account and, after extracting the correct exponential phase, expand around $\mathbf{q} - \mathbf{p}_M = \mathbf{0}$ to simplify the calculation. For instance, we have

$$I_1^{(a)}(\{x\}, z_{12}) = e^{i \frac{x_3}{x_1+x_2} (x_1 \mathbf{z}_1 + x_2 \mathbf{z}_2) \cdot (\mathbf{q} - \mathbf{p}_M)} \times \frac{2\pi}{x_3(x_1+x_2)} K_0 \left(\sqrt{\frac{x_1 x_2}{x_1+x_2} Q^2 z_{12}^2} \sqrt{1 + \frac{(\mathbf{q} - \mathbf{p}_M)^2}{x_3(x_1+x_2) Q^2}} \right) , \quad (\text{C.7})$$

that can be simplified to

$$\left. \frac{I_1^{(a)}(\{x\}, z_{12})}{e^{i \frac{x_3}{x_1+x_2} (x_1 \mathbf{z}_1 + x_2 \mathbf{z}_2) \cdot (\mathbf{q} - \mathbf{p}_M)}} \right|_{\text{f.}} = \frac{2\pi}{x_3(x_1+x_2)} K_0 \left(\sqrt{\frac{x_1 x_2}{x_1+x_2} Q^2 z_{12}^2} \right) \equiv \frac{2\pi}{x_3} F_1(x_1, x_2, z_{12}^2) , \quad (\text{C.8})$$

observing that this integral enters the $T \rightarrow T$ transition. Please note that, for the transverse-momentum integrals, we introduce the notations $|_{\text{F.}}$ (forward) and $|_{\text{n.F.}}$ (next-to-forward) to indicate the level of accuracy at which the integral is evaluated in the $\mathbf{q} - \mathbf{p}_M$ expansion around zero. Moreover, n.F. is also employed as a superscript of some functions appearing in the next-to-forward approximation. This notation should not be confused with the notions of flip (f.) and non-flip (n.f.). This observation is particularly useful for obtaining fully integrated forms for I_2 and I_3 , which read

$$\begin{aligned} \left. \frac{I_2^{(a)}(\{x\}, z_{12})}{e^{i \frac{x_3}{x_1+x_2} (x_1 \mathbf{z}_1 + x_2 \mathbf{z}_2) \cdot (\mathbf{q} - \mathbf{p}_M)}} \right|_{\text{n.F.}} &= \frac{2\pi}{x_3} \left\{ \frac{z_{12\perp\nu}}{x_1 z_{12}^2 Q^2} \left[\sqrt{\frac{x_1 x_2}{x_1+x_2} z_{12}^2 Q^2} K_1 \left(\sqrt{\frac{x_1 x_2}{x_1+x_2} z_{12}^2 Q^2} \right) \right. \right. \\ &\quad \left. \left. - \sqrt{x_1 \bar{x}_1} Q^2 z_{12}^2 K_1 \left(\sqrt{x_1 \bar{x}_1} Q^2 z_{12}^2 \right) \right] + \frac{x_3}{Q^2} \left[\frac{z_{12\perp\nu} i(q - p_M)_\perp \cdot z_{12\perp}}{z_{12}^2} \frac{\sqrt{x_1 \bar{x}_1} Q^2 z_{12}^2}{(x_1+x_2)} \right. \right. \\ &\quad \left. \left. \times K_1 \left(\sqrt{x_1 \bar{x}_1} Q^2 z_{12}^2 \right) + \left(i(p_M - q)_\perp - 2z_{12\perp\nu} \frac{i(q - p_M)_\perp \cdot z_{12\perp}}{z_{12}^2} \right) \right. \right. \\ &\quad \left. \left. \times \left(\frac{x_2}{(x_1+x_2)x_1 x_3} K_1 \left(\sqrt{\frac{x_1 x_2}{x_1+x_2} z_{12}^2} \right) - \frac{x_2+x_3}{x_1 x_2} K_2 \left(\sqrt{x_1 \bar{x}_1} Q^2 z_{12}^2 \right) \right) \right] \right\} \end{aligned}$$

$$\begin{aligned} &\equiv \frac{2\pi}{x_3} \left\{ z_{12\perp\nu} F_2(x_1, x_2, \mathbf{z}_{12}^2) + z_{12\perp\nu} i(q - p_M)_\perp \cdot z_{12\perp} F_2^{\text{n.F.}}(x_1, x_2, \mathbf{z}_{12}^2) \right. \\ &\quad \left. - (z_{12}^2 i(q - p_M)_\perp\nu + 2z_{12\perp\nu} i(q - p_M)_\perp \cdot z_{12\perp}) \tilde{F}_2^{\text{n.F.}}(x_1, x_2, \mathbf{z}_{12}^2) \right\} \quad (\text{C.9}) \end{aligned}$$

and

$$\begin{aligned} &\frac{I_3^{(a)}(\{x\}, z_{12})}{e^{i\frac{x_3}{x_1+x_2}(x_1 z_1 + x_2 z_2)(q-p_M)} \Big|_{\text{F.}}} = -\frac{2\pi}{x_1 x_3 Q^2 \mathbf{z}_{12}^2} \left(g_{\perp\alpha\nu} + \frac{2z_{12\perp\nu} z_{12\perp\alpha}}{\mathbf{z}_{12}^2} \right) \\ &\times \left[\sqrt{x_1 \bar{x}_1 Q^2 \mathbf{z}_{12}^2} K_1 \left(\sqrt{x_1 \bar{x}_1 Q^2 \mathbf{z}_{12}^2} \right) - \sqrt{\frac{x_1 x_2}{x_1 + x_2} Q^2 \mathbf{z}_{12}^2} K_1 \left(\sqrt{\frac{x_1 x_2}{x_1 + x_2} Q^2 \mathbf{z}_{12}^2} \right) \right] \\ &- \frac{2\pi}{x_1 x_3} \frac{z_{12\perp\nu} z_{12\perp\alpha}}{\mathbf{z}_{12}^2} \left[x_1 \bar{x}_1 K_0 \left(\sqrt{x_1 \bar{x}_1 Q^2 \mathbf{z}_{12}^2} \right) - \frac{x_1 x_2}{x_1 + x_2} K_0 \left(\sqrt{\frac{x_1 x_2}{x_1 + x_2} Q^2 \mathbf{z}_{12}^2} \right) \right] \\ &= \frac{2\pi}{x_3} \left[\left(g_{\perp\alpha\nu} + \frac{2z_{12\perp\nu} z_{12\perp\alpha}}{\mathbf{z}_{12}^2} \right) F_3(x_1, x_2, \mathbf{z}_{12}^2) + \frac{z_{12\perp\nu} z_{12\perp\alpha}}{\mathbf{z}_{12}^2} \tilde{F}_3(x_1, x_2, \mathbf{z}_{12}^2) \right]. \quad (\text{C.10}) \end{aligned}$$

We observe that, in the first integral, we kept a next-to-forward accuracy in order to get a non-zero contribution to the s -channel non-conserving helicity amplitude. We observe that we can greatly simplify the expression of the longitudinal-photon-to-transverse-meson amplitude by observing that

$$\int_0^{2\pi} d\varphi \left(2(\boldsymbol{\varepsilon}_M^* \cdot \mathbf{r})(\mathbf{r} \cdot \boldsymbol{\Delta}) - (\boldsymbol{\varepsilon}_M^* \cdot \boldsymbol{\Delta}) r^2 \right) = 0,$$

where φ is the angle associated to the vector \mathbf{r} . This implies that the structure $\tilde{F}_2^{\text{n.f.}}$ will not contribute.

Performing the integrals and the tensor contraction and making the change of variables in (C.6), we can finally obtain

$$\begin{aligned} \mathcal{A}_3^{(a)T,L} &= (2\pi)^4 W^2 \delta^{(4)}(q + p_t - p_M - p_{t'}) \left(\prod_{i=1}^3 \int_0^1 dx_i \right) \delta \left(1 - \sum_i x_i \right) \int d^2\mathbf{r} \mathcal{U}(\mathbf{r}) \\ &\quad \times \left(-\frac{e_q m_M}{\pi} Q^2 (\mathbf{r} \cdot \boldsymbol{\Delta}) \right) \left[\frac{\varepsilon_\gamma^+}{q^+} (\boldsymbol{\varepsilon}_M^* \cdot \mathbf{r}) \right] \left\{ (1 - c_f) \phi_{3L}(x_1, x_2) \right. \\ &\quad \left. \times \left(\frac{x_1^2}{x_3(x_1 + x_2)} F_2(x_1, x_2, \mathbf{r}^2) - \frac{x_1}{x_3} F_2^{\text{n.F.}}(x_1, x_2, \mathbf{r}^2) \right) + (x_1 \leftrightarrow x_2) \right\} \quad (\text{C.11}) \end{aligned}$$

for the $L \rightarrow T$ transition and

$$\begin{aligned} \mathcal{A}_3^{(a)T,T} &= (2\pi)^4 W^2 \delta^{(4)}(q + p_t - p_M - p_{t'}) \left(\prod_{i=1}^3 \int_0^1 dx_i \right) \delta \left(1 - \sum_i x_i \right) \int d^2\mathbf{r} \mathcal{U}(\mathbf{r}) \\ &\times \left(-\frac{e_q m_M}{8\pi} \right) (1 - c_f) \left\{ \frac{8}{x_3^2} T_{\text{f.}}(\mathbf{r}) \left(2F_3(x_1, x_2, \mathbf{r}) + \tilde{F}_3(x_1, x_2, \mathbf{r}) \right) \phi_{3,(+)}(x_1, x_2) - \frac{4}{x_3} T_{\text{n.f.}}(\mathbf{r}) \right. \\ &\quad \left. \times \left[\frac{x_1 x_2}{1 - x_2} F_1(x_1, x_2, \mathbf{r}) \phi_{3,(-)}(x_1, x_2) \right] \right\} \end{aligned}$$

$$+ \frac{\tilde{F}_3(x_1, x_2, \mathbf{r})}{(1-x_1)x_3} \left(x_1 \phi_{3,(+)}(x_1, x_2) - (1-2x_1)\phi_{3,(-)}(x_1, x_2) \right) \Big] + (x_1 \leftrightarrow x_2) \Big\} \quad (\text{C.12})$$

for the $T \rightarrow T$ transition, where we introduced the combination of DAs

$$\phi_{3,L}(x_1, x_2) = f_{3M}^A A(x_1, x_2) - \left(1 + \frac{2x_2}{x_3} \right) f_{3M}^V V(x_1, x_2), \quad (\text{C.13})$$

$$\phi_{3,(+)}(x_1, x_2) = (x_1 + x_2) f_{3M}^A A(x_1, x_2) + (x_2 - x_1) f_{3M}^V V(x_1, x_2), \quad (\text{C.14})$$

$$\phi_{3,(-)}(x_1, x_2) = (f_{3M}^V V(x_1, x_2) - f_{3M}^A A(x_1, x_2)). \quad (\text{C.15})$$

C.2 $\mathcal{U}_{z_1 z_3}$ plus $\mathcal{U}_{z_3 z_2}$ -part of the amplitude

It is convenient to consider the gluon-quark dipoles simultaneously:

$$\begin{aligned} \mathcal{A}_3^{(b)} = & - \left(\prod_{i=1}^3 \int_0^1 dx_i \right) \delta \left(1 - \sum_i x_i \right) \frac{e_q m_M}{8\pi} c_f \left(\varepsilon_{q\rho} - \frac{\varepsilon_q^+}{q^+} q_\rho \right) \left(\varepsilon_M^{*\mu} - \frac{p_M^\mu}{p_M^+} \varepsilon_M^{*+} \right) \delta \left(1 - \frac{p_M^+}{q^+} \right) \\ & \times \left\{ \int d^2 \mathbf{z}_1 d^2 \mathbf{z}_3 e^{i(\mathbf{q}-\mathbf{p}_M)(x_1 \mathbf{z}_1 + x_3 \mathbf{z}_3)} \langle P(p') | \mathcal{U}_{z_1 z_3} | P(p) \rangle \int d^2 \mathbf{z}_2 e^{ix_2(\mathbf{q}-\mathbf{p}_M)\mathbf{z}_2} \Psi_3(\{x\}, \{\mathbf{z}\}) \right. \\ & \left. + \int d^2 \mathbf{z}_2 d^2 \mathbf{z}_3 e^{i(\mathbf{q}-\mathbf{p}_M)(x_2 \mathbf{z}_2 + x_3 \mathbf{z}_3)} \langle P(p') | \mathcal{U}_{z_3 z_2} | P(p) \rangle \int d^2 \mathbf{z}_1 e^{ix_1(\mathbf{q}-\mathbf{p}_M)\mathbf{z}_1} \Psi_3(\{x\}, \{\mathbf{z}\}) \right\}. \end{aligned} \quad (\text{C.16})$$

In the second term (last line), if we make the relabelling $\mathbf{z}_2 \leftrightarrow \mathbf{z}_1$ and use the property

$$\Psi_3(x_1, x_2, x_3, \mathbf{z}_2, \mathbf{z}_1, \mathbf{z}_3) = \Psi_3(x_2, x_1, x_3, \mathbf{z}_1, \mathbf{z}_2, \mathbf{z}_3), \quad (\text{C.17})$$

we obtain

$$\begin{aligned} \mathcal{A}_3^{(b)} = & - \left(\prod_{i=1}^3 \int_0^1 dx_i \right) \delta \left(1 - \sum_i x_i \right) \frac{e_q m_M}{8\pi} c_f \left(\varepsilon_{q\rho} - \frac{\varepsilon_q^+}{q^+} q_\rho \right) \left(\varepsilon_M^{*\mu} - \frac{p_M^\mu}{p_M^+} \varepsilon_M^{*+} \right) \delta \left(1 - \frac{p_M^+}{q^+} \right) \\ & \times \int d^2 \mathbf{z}_1 d^2 \mathbf{z}_3 \left\{ e^{i(\mathbf{q}-\mathbf{p}_M)(x_1 \mathbf{z}_1 + x_3 \mathbf{z}_3)} \langle P(p') | \mathcal{U}_{z_1 z_3} | P(p) \rangle \Psi_3^{(b)}(x_1, x_2, x_3, \mathbf{z}_{13}) \right. \\ & \left. + e^{i(\mathbf{q}-\mathbf{p}_M)(x_2 \mathbf{z}_1 + x_3 \mathbf{z}_3)} \langle P(p') | \mathcal{U}_{z_3 z_1} | P(p) \rangle \Psi_3^{(b)}(x_2, x_1, x_3, \mathbf{z}_{13}) \right\}, \end{aligned} \quad (\text{C.18})$$

where

$$\begin{aligned} \Psi_3^{(b)}(\{x\}, \mathbf{z}_{13}) = & \int d^2 \mathbf{z}_2 e^{ix_2(\mathbf{q}-\mathbf{p}_M)\mathbf{z}_2} \left\{ f_{3M}^V g_{\sigma\mu} V(x_1, x_2) \left[\left(4g_\perp^{\rho\sigma} \frac{x_1 x_2}{1-x_2} \frac{Q}{Z} K_1(QZ) \right. \right. \right. \\ & \left. \left. - 4i \left[2x_1 q^\rho \left(2 \frac{x_2}{x_3} + 1 \right) g_\perp^{\sigma\nu} - \Xi_1^{\alpha\nu\rho\sigma} i \partial_{z_{1\perp}\alpha} \right] \frac{z_{23\perp\nu}}{z_{23}^2} K_0(QZ) \right] - (1 \leftrightarrow 2) \right] \\ & \left. - \epsilon_{-\sigma\beta} f_{3M}^A g_{\perp\mu}^\beta A(x_1, x_2) \left[\left(4\epsilon^{\sigma\rho+} \frac{x_1 x_2}{1-x_2} \frac{Q}{Z} K_1(QZ) \right. \right. \right. \end{aligned}$$

$$+\frac{4i}{\bar{x}_1} \left[2x_1 \bar{x}_1 q^\rho \epsilon^{\nu\sigma+-} - \Xi_2^{\alpha\nu\rho\sigma} i \partial_{z_{1\perp}\alpha} \right] \frac{z_{23\perp\nu}}{z_{23}^2} K_0(QZ) + (1 \leftrightarrow 2) \Big] \Big\}. \quad (\text{C.19})$$

Since the dipole matrix element depends on the relative distance vector \mathbf{z}_{13} , it is clear that the second contribution is obtained from the first through the exchange $(x_1, x_2, \mathbf{z}_{13}) \rightarrow (x_2, x_1, -\mathbf{z}_{13})$. Thus, we can write

$$\begin{aligned} \mathcal{A}_3^{(b)} = & - \left(\prod_{i=1}^3 \int_0^1 dx_i \right) \delta \left(1 - \sum_i x_i \right) \frac{e_q m_M}{8\pi} c_f \left(\varepsilon_{q\rho} - \frac{\varepsilon_q^+}{q^+} q_\rho \right) \left(\varepsilon_M^{*\mu} - \frac{p_M^\mu}{p_M^+} \varepsilon_M^{*+} \right) \delta \left(1 - \frac{p_M^+}{q^+} \right) \\ & \times \int d^2 \mathbf{z}_1 d^2 \mathbf{z}_3 \langle P(p') | \mathcal{U}_{\mathbf{z}_1 \mathbf{z}_3} | P(p) \rangle \left\{ e^{i(\mathbf{q}-\mathbf{p}_M)(x_1 \mathbf{z}_1 + x_3 \mathbf{z}_3)} \Psi_3^{(b)}(x_1, x_2, x_3, \mathbf{z}_{13}) \right. \\ & \left. + (x_1 \leftrightarrow x_2, \mathbf{z}_{13} \rightarrow -\mathbf{z}_{13}) \right\}. \end{aligned} \quad (\text{C.20})$$

Since we integrate over \mathbf{z}_2 , it is clear that the symmetry $(1 \leftrightarrow 2)$ within the function $\Psi_3^{(b)}$ is not preserved. To integrate all terms explicitly we need the following integrals:

$$I_1^{(b)}(\{x\}, z_{13}) = \int d^2 \mathbf{z}_2 e^{ix_2(\mathbf{q}-\mathbf{p}_M)\mathbf{z}_2} \frac{Q}{Z} K_1(QZ), \quad (\text{C.21})$$

$$I_2^{(b)}(\{x\}, z_{13}) = \int d^2 \mathbf{z}_2 e^{ix_2(\mathbf{q}-\mathbf{p}_M)\mathbf{z}_2} \frac{z_{23\perp\nu}}{z_{23}^2} K_0(QZ), \quad (\text{C.22})$$

$$I_3^{(b)}(\{x\}, z_{13}) = \int d^2 \mathbf{z}_2 e^{ix_2(\mathbf{q}-\mathbf{p}_M)\mathbf{z}_2} \frac{z_{23\perp\nu}}{z_{23}^2} \frac{\partial}{\partial z_{1\perp}^\alpha} K_0(QZ) = \frac{\partial}{\partial z_{1\perp}^\alpha} I_1^{(b)}(\{x\}, z_{12}), \quad (\text{C.23})$$

$$I_4^{(b)}(\{x\}, z_{13}) = \int d^2 \mathbf{z}_2 e^{ix_2(\mathbf{q}-\mathbf{p}_M)\mathbf{z}_2} K_0(QZ). \quad (\text{C.24})$$

The first three integrals can be obtained from the ones in eqs. (C.3), (C.4), (C.5), under suitable exchanges of pair of variables (x_i, \mathbf{z}_i) . The absence of the integral

$$\int d^2 \mathbf{z}_2 e^{ix_2(\mathbf{q}-\mathbf{p}_M)\mathbf{z}_2} \frac{z_{13\perp\nu}}{z_{13}^2} \frac{\partial}{\partial z_{2\perp}^\alpha} K_0(QZ) \quad (\text{C.25})$$

is due to the fact that the latter starts at next-to-forward accuracy and enters the $T \rightarrow T$ transition, thus being subleading in this helicity amplitude. The integrals in eqs. (C.21), (C.22), (C.23) and (C.24) read

$$\frac{I_1^{(b)}(\{x\}, z_{13})}{e^{i\frac{x_2}{x_1+x_3}(x_1 \mathbf{z}_1 + x_3 \mathbf{z}_3)(\mathbf{q}-\mathbf{p}_M)}} \Big|_{\text{F.}} = \frac{2\pi}{x_2(x_1+x_3)} K_0 \left(\sqrt{\frac{x_1 x_3}{x_1+x_3} Q^2 z_{13}^2} \right) \equiv \frac{2\pi}{x_2} F_1(x_1, x_3, \mathbf{z}_{13}^2), \quad (\text{C.26})$$

$$\frac{I_2^{(b)}(\{x\}, z_{13})}{e^{i\frac{x_2}{x_1+x_3}(x_1 \mathbf{z}_1 + x_3 \mathbf{z}_3)(\mathbf{q}-\mathbf{p}_M)}} \Big|_{\text{n.F.}} = -\frac{2\pi}{x_2} \left\{ \frac{z_{13\perp\nu}}{x_1 z_{13}^2 Q^2} \left[\sqrt{\frac{x_1 x_3}{x_1+x_3} z_{13}^2 Q^2} K_1 \left(\sqrt{\frac{x_1 x_3}{x_1+x_3} z_{13}^2 Q^2} \right) \right. \right.$$

$$\begin{aligned}
& -\sqrt{x_1\bar{x}_1Q^2z_{13}^2}K_1\left(\sqrt{x_1\bar{x}_1Q^2z_{13}^2}\right)\Bigg] + \frac{x_2}{Q^2}\left[\frac{z_{13\perp\nu}i(q-p_M)_\perp\cdot z_{13\perp}}{z_{13}^2}\frac{\sqrt{x_1\bar{x}_1Q^2z_{13}^2}}{(x_1+x_3)}\right. \\
& \quad \times K_1\left(\sqrt{x_1\bar{x}_1Q^2z_{13}^2}\right) + \left(i(p_M-q)_\perp - 2z_{13\perp\nu}\frac{i(q-p_M)_\perp\cdot z_{13\perp}}{z_{13}^2}\right) \quad (C.27)
\end{aligned}$$

$$\begin{aligned}
& \times \left(\frac{x_3}{(x_1+x_3)x_1x_2}K_1\left(\sqrt{\frac{x_1x_3Q^2z_{13}^2}{x_1+x_3}}\right) - \frac{x_2+x_3}{x_1x_3}K_2\left(\sqrt{x_1\bar{x}_1Q^2z_{13}^2}\right)\right)\Bigg] \\
& \equiv -\frac{2\pi}{x_2}\left\{z_{13\perp\nu}F_2(x_1, x_3, z_{13}^2) + z_{13\perp\nu}i(q-p_M)_\perp\cdot z_{13\perp}F_2^{\text{n.F.}}(x_1, x_3, z_{13}^2)\right. \\
& \quad \left. - (z_{13}^2i(q-p_M)_\perp\nu + 2z_{13\perp\nu}i(q-p_M)_\perp\cdot z_{13\perp})\tilde{F}_2^{\text{n.F.}}(x_1, x_3, z_{13}^2)\right\}, \quad (C.28)
\end{aligned}$$

$$\begin{aligned}
& \frac{I_3^{(b)}(\{x\}, z_{13})}{e^{i\frac{x_2}{x_1+x_3}(x_1z_1+x_3z_3)(q-p_M)}\Big|_{\text{F.}}} = \frac{2\pi}{x_1x_2Q^2z_{13}^2}\left(g_{\perp\alpha\nu} + \frac{2z_{13\perp\nu}z_{13\perp\alpha}}{z_{13}^2}\right) \\
& \times \left[\sqrt{x_1\bar{x}_1Q^2z_{13}^2}K_1\left(\sqrt{x_1\bar{x}_1Q^2z_{13}^2}\right) - \sqrt{\frac{x_1x_3}{x_1+x_3}Q^2z_{13}^2}K_1\left(\sqrt{\frac{x_1x_3}{x_1+x_3}Q^2z_{13}^2}\right)\right] \\
& + \frac{2\pi}{x_1x_2}\frac{z_{13\perp\nu}z_{13\perp\alpha}}{z_{13}^2}\left[x_1\bar{x}_1K_0\left(\sqrt{x_1\bar{x}_1Q^2z_{13}^2}\right) - \frac{x_1x_3}{x_1+x_3}K_0\left(\sqrt{\frac{x_1x_3}{x_1+x_3}Q^2z_{13}^2}\right)\right] \\
& = -\frac{2\pi}{x_2}\left[\left(g_{\perp\alpha\nu} + \frac{2z_{13\perp\nu}z_{13\perp\alpha}}{z_{13}^2}\right)F_3(x_1, x_3, z_{13}^2) + \frac{z_{13\perp\nu}z_{13\perp\alpha}}{z_{13}^2}\tilde{F}_3(x_1, x_3, z_{13}^2)\right], \quad (C.29)
\end{aligned}$$

$$\begin{aligned}
& \frac{I_4^{(b)}(\{x\}, z_{13})}{e^{i\frac{x_2}{x_1+x_3}(x_1z_1+x_3z_3)(q-p_M)}} = \frac{2\pi}{x_2(x_1+x_3)Q^2}\sqrt{\frac{x_1x_3}{x_1+x_3}z_{13}^2Q^2} \\
& \times \frac{K_1\left(\sqrt{\frac{x_1x_3}{x_1+x_3}Q^2z_{13}^2}\sqrt{1+\frac{x_2}{x_1+x_3}\frac{(q-p_M)^2}{Q^2}}\right)}{\sqrt{1+\frac{x_2}{x_1+x_3}\frac{(q-p_M)^2}{Q^2}}} \equiv \frac{2\pi}{x_2}z_{13}^2F_4(x_1, x_3, z_{13}^2). \quad (C.30)
\end{aligned}$$

Armed with these integrals and performing the change of variables¹⁰

$$\mathbf{r} = \mathbf{z}_1 - \mathbf{z}_3, \quad \mathbf{b} = \frac{x_1\mathbf{z}_1 + x_3\mathbf{z}_3}{x_1 + x_3}, \quad (C.31)$$

we get

$$\begin{aligned}
\mathcal{A}_3^{(b)T,L} & = (2\pi)^4 W^2 \delta^{(4)}(q + p_t - p_M - p_{t'}) \left(\prod_{i=1}^3 \int_0^1 dx_i\right) \delta\left(1 - \sum_i x_i\right) \int d^2\mathbf{r} \mathcal{U}(\mathbf{r}) \\
& \quad \times \left[-\frac{e_q m_M}{\pi} Q^2 (\mathbf{r} \cdot \boldsymbol{\Delta})\right] \left[(\boldsymbol{\varepsilon}_M^* \cdot \mathbf{r}) \frac{\varepsilon_\gamma^+}{q^+}\right] \left\{c_f \phi_{3L}(x_1, x_2)\right. \\
& \quad \times \left(\frac{x_1 F_2^{\text{n.F.}}(x_1, x_3, \mathbf{r}^2)}{x_2} - \frac{x_1^2 F_2(x_1, x_3, \mathbf{r}^2)}{x_2(x_1+x_3)} + \frac{x_2 F_4(x_2, x_3, \mathbf{r}^2)}{x_2+x_3}\right) + (x_1 \leftrightarrow x_2)\Big\} \quad (C.32)
\end{aligned}$$

¹⁰Please note that after this change of variable it is evident that the transformation $(x_1 \leftrightarrow x_2, z_{13} \rightarrow -z_{13})$ is equivalent to the $(1 \leftrightarrow 2)$ one.

and

$$\begin{aligned}
\mathcal{A}_3^{(b)T,T} &= (2\pi)^4 W^2 \delta^{(4)}(q + p_t - p_M - p_{t'}) \left(\prod_{i=1}^3 \int_0^1 dx_i \right) \delta \left(1 - \sum_i x_i \right) \int d^2 \mathbf{r} \mathcal{U}(\mathbf{r}) \\
&\times \left(-\frac{e_q m_M}{8\pi} \right) c_f \left\{ -\frac{8}{x_2 x_3} T_{\text{f.}}(\mathbf{r}) \left(2F_3(x_1, x_3, \mathbf{r}) + \tilde{F}_3(x_1, x_3, \mathbf{r}) \right) \phi_{3,(+)}(x_1, x_2) - 4 T_{\text{n.f.}}(\mathbf{r}) \right. \\
&\quad \times \left[\frac{x_1 x_2}{(1-x_1)(1-x_2)} F_1(x_1, x_3, \mathbf{r}) \left(\frac{\phi_{3,(+)}(x_1, x_2)}{x_2} - \frac{2}{x_2} f_M^A A(x_1, x_2) \right) \right. \\
&\quad \quad \left. + \frac{2F_3(x_1, x_3, \mathbf{r})}{(1-x_1)x_2 x_3} \left(-(1-2x_1)\phi_{3,(-)}(x_1, x_2) + \phi_{3,(+)}(x_1, x_2) \right) \right. \\
&\quad \left. \left. + \frac{\tilde{F}_3(x_1, x_3, \mathbf{r})}{(1-x_1)x_2 x_3} \left(-x_1 \phi_{3,(+)}(x_1, x_2) + (1-2x_1)\phi_{3,(-)}(x_1, x_2) \right) \right] + (x_1 \leftrightarrow x_2) \right\}. \quad (\text{C.33})
\end{aligned}$$

In the present form, it is not immediate that the result can be expressed in terms of only the independent combinations of DAs $\phi_{3,(\pm)}$. However, by manipulating the proportional term to $A(x_1, x_2)$, as follows:

$$\begin{aligned}
&\left(\prod_{i=1}^3 \int_0^1 dx_i \right) \delta \left(1 - \sum_i x_i \right) \dots \left(\frac{x_1 x_2}{(1-x_1)(1-x_2)} \right) \left[\frac{2F_1(x_1, x_3, \mathbf{r}^2)}{x_2} f_{3M}^A A(x_1, x_2) \right] \\
&= \left(\prod_{i=1}^3 \int_0^1 dx_i \right) \delta \left(1 - \sum_i x_i \right) \dots \left(\frac{x_1 x_2}{(1-x_1)(1-x_2)} \right) \\
&\quad \times \left[-\frac{x_2 F_1(x_2, x_3, \mathbf{r}^2) + x_1 F_1(x_1, x_3, \mathbf{r}^2)}{x_1 x_2} \right] \phi_{3,(-)}(x_1, x_2), \quad (\text{C.34})
\end{aligned}$$

we obtain

$$\begin{aligned}
\mathcal{A}_3^{(b)T,T} &= (2\pi)^4 W^2 \delta^{(4)}(q + p_t - p_M - p_{t'}) \left(\prod_{i=1}^3 \int_0^1 dx_i \right) \delta \left(1 - \sum_i x_i \right) \int d^2 \mathbf{r} \mathcal{U}(\mathbf{r}) \\
&\times \left(-\frac{e_q m_M}{8\pi} \right) c_f \left\{ -\frac{8}{x_2 x_3} T_{\text{f.}}(\mathbf{r}) \left(2F_3(x_1, x_3, \mathbf{r}) + \tilde{F}_3(x_1, x_3, \mathbf{r}) \right) \phi_{3,(+)}(x_1, x_2) - 4 T_{\text{n.f.}}(\mathbf{r}) \right. \\
&\quad \times \left[\frac{x_1 x_2}{(1-x_1)(1-x_2)} \left(\frac{\phi_{3,(+)}(x_1, x_2)}{x_2} F_1(x_1, x_3, \mathbf{r}) \right. \right. \\
&\quad \quad \left. \left. + \frac{x_2 F_1(x_2, x_3, \mathbf{r}^2) + x_1 F_1(x_1, x_3, \mathbf{r}^2)}{x_1 x_2} \phi_{3,(-)}(x_1, x_2) \right) \right. \\
&\quad \left. \left. - \frac{\tilde{F}_3(x_1, x_3, \mathbf{r})}{(1-x_1)x_2 x_3} \left(x_1 \phi_{3,(+)}(x_1, x_2) - (1-2x_1)\phi_{3,(-)}(x_1, x_2) \right) \right] + (x_1 \leftrightarrow x_2) \right\}. \quad (\text{C.35})
\end{aligned}$$

C.3 Full result for $\mathcal{A}_3^{T,L}$ and $\mathcal{A}_3^{T,T}$

Combining the results of Appendices C.1 and C.2, for the longitudinal-photon-to-transverse-meson amplitude, we obtain

$$\mathcal{A}_3^{T,L} = (2\pi)^4 W^2 \delta^{(4)}(q + p_t - p_M - p_{t'}) \left(\prod_{i=1}^3 \int_0^1 dx_i \right) \delta \left(1 - \sum_i x_i \right) \int d^2 \mathbf{r} \mathcal{U}(\mathbf{r}) (\mathbf{r} \cdot \mathbf{\Delta})$$

$$\begin{aligned}
& \times \tau_L \left[(\boldsymbol{\varepsilon}_M^* \cdot \mathbf{r}) \frac{\varepsilon_\gamma^+}{q^+} \right] \left\{ \phi_{3L}(x_1, x_2) \left[(1 - c_f) \left(\frac{x_1^2}{x_3(x_1 + x_2)} F_2(x_1, x_2, \mathbf{r}^2) - \frac{x_1 F_2^{\text{n.F.}}(x_1, x_2, \mathbf{r}^2)}{x_3} \right) \right. \right. \\
& \left. \left. + c_f \left(\frac{x_1 F_2^{\text{n.F.}}(x_1, x_3, \mathbf{r}^2)}{x_2} - \frac{x_1^2 F_2(x_1, x_3, \mathbf{r}^2)}{x_2(x_1 + x_3)} + \frac{x_2 F_4(x_2, x_3, \mathbf{r}^2)}{x_2 + x_3} \right) \right] + (x_1 \leftrightarrow x_2) \right\}, \tag{C.36}
\end{aligned}$$

where $\tau_L = -e_q m_M Q^2 / \pi$. Similarly, the full result for the transverse-photon-to-transverse-meson amplitude reads

$$\begin{aligned}
\mathcal{A}_3^{(b)T,T} &= (2\pi)^4 W^2 \delta^{(4)}(q + p_t - p_M - p_{t'}) \left(\prod_{i=1}^3 \int_0^1 dx_i \right) \delta \left(1 - \sum_i x_i \right) \int d^2 \mathbf{r} \mathcal{U}(\mathbf{r}) \\
& \times \tau_T \left\{ T_{\text{f.}}(\mathbf{r}) 2 \left(c_f \frac{2F_3(x_1, x_3, \mathbf{r}) + \tilde{F}_3(x_1, x_3, \mathbf{r})}{x_2 x_3} - (1 - c_f) \frac{2F_3(x_1, x_2, \mathbf{r}) + \tilde{F}_3(x_1, x_2, \mathbf{r})}{x_3^2} \right) \right. \\
& \quad \times \phi_{3,(+)}(x_1, x_2) + T_{\text{n.f.}}(\mathbf{r}) \left[\frac{x_1 x_2}{(1 - x_2)} \left(c_f \left(\frac{\phi_{3,(+)}(x_1, x_2)}{(1 - x_1)x_2} F_1(x_1, x_3, \mathbf{r}) \right. \right. \right. \\
& \quad \left. \left. + \frac{x_2 F_1(x_2, x_3, \mathbf{r}^2) + x_1 F_1(x_1, x_3, \mathbf{r}^2)}{(1 - x_1)x_1 x_2} \phi_{3,(-)}(x_1, x_2) \right) + (1 - c_f) \frac{F_1(x_1, x_2, \mathbf{r})}{x_3} \phi_{3,(-)}(x_1, x_2) \right) \\
& \quad \left. + \left(\frac{(1 - c_f) \tilde{F}_3(x_1, x_2, \mathbf{r})}{(1 - x_1)x_3^2} - \frac{c_f \tilde{F}_3(x_1, x_3, \mathbf{r})}{(1 - x_1)x_3 x_2} \right) \left(x_1 \phi_{3,(+)}(x_1, x_2) - (1 - 2x_1) \phi_{3,(-)}(x_1, x_2) \right) \right] \\
& \quad \left. + (x_1 \leftrightarrow x_2) \right\}, \tag{C.37}
\end{aligned}$$

where $\tau_T = e_q m_M / 2\pi$.

C.4 Summary of $F_i(x_i, x_j, \mathbf{r}^2)$ and $\tilde{F}_i(x_i, x_j, \mathbf{r}^2)$'s functions

For the convenience of the reader, we report here all the $F_i(x_i, x_j, \mathbf{r}^2)$ and $\tilde{F}_i(x_i, x_j, \mathbf{r}^2)$ functions appearing in the final results of the previous section:

$$F_1(x_i, x_j, \mathbf{r}^2) = \frac{1}{(x_i + x_j)} K_0 \left(\sqrt{\frac{x_i x_j}{x_i + x_j} Q^2 \mathbf{r}^2} \right), \tag{C.38}$$

$$F_2(x_i, x_j, \mathbf{r}^2) = \sqrt{\frac{\bar{x}_i}{x_i Q^2 \mathbf{r}^2}} K_1 \left(\sqrt{x_i \bar{x}_i Q^2 \mathbf{r}^2} \right) - \sqrt{\frac{x_j}{x_i(x_i + x_j) Q^2 \mathbf{r}^2}} K_1 \left(\sqrt{\frac{x_i x_j}{x_i + x_j} Q^2 \mathbf{r}^2} \right), \tag{C.39}$$

$$F_2^{\text{n.F.}}(x_i, x_j, \mathbf{r}^2) = \frac{(1 - x_i - x_j)}{(x_i + x_j)} \sqrt{\frac{x_i \bar{x}_i}{Q^2 \mathbf{r}^2}} K_1 \left(\sqrt{x_i \bar{x}_i Q^2 \mathbf{r}^2} \right), \tag{C.40}$$

$$\begin{aligned}
& \tilde{F}_2^{\text{n.F.}}(x_i, x_j, \mathbf{r}^2) = \frac{1}{Q^2 \mathbf{r}^2 x_i} \\
& \times \left(\frac{x_j}{(x_i + x_j)} K_1 \left(\sqrt{\frac{x_i x_j Q^2 \mathbf{r}^2}{x_i + x_j}} \right) - \frac{(1 - x_i - x_j)(1 - x_i)}{x_j} K_2 \left(\sqrt{x_i \bar{x}_i Q^2 \mathbf{r}^2} \right) \right), \tag{C.41}
\end{aligned}$$

$$F_3(x_i, x_j, \mathbf{r}^2) = \sqrt{\frac{\bar{x}_i}{x_i Q^2 \mathbf{r}^2}} K_1\left(\sqrt{x_i \bar{x}_i Q^2 \mathbf{r}^2}\right) - \sqrt{\frac{x_j}{x_i(x_i + x_j) Q^2 \mathbf{r}^2}} K_1\left(\sqrt{\frac{x_i x_j}{x_i + x_j} Q^2 \mathbf{r}^2}\right), \quad (\text{C.42})$$

$$\tilde{F}_3(x_i, x_j, \mathbf{r}^2) = \bar{x}_i K_0\left(\sqrt{x_i \bar{x}_i Q^2 \mathbf{r}^2}\right) - \frac{x_j}{x_i + x_j} K_0\left(\sqrt{\frac{x_i x_j}{x_i + x_j} Q^2 \mathbf{r}^2}\right) \quad (\text{C.43})$$

and

$$\begin{aligned} F_4(x_i, x_j, \mathbf{r}^2) &= \frac{1}{(x_i + x_j) Q^2 \mathbf{r}^2} \sqrt{\frac{x_i x_j}{(x_i + x_j)} Q^2 \mathbf{r}^2} \\ &\times \frac{K_1\left(\sqrt{\frac{x_i x_j}{(x_i + x_j)} Q^2 \mathbf{r}^2} \sqrt{1 + \frac{(1 - x_i - x_j) \Delta^2}{(x_i + x_j) Q^2}}\right)}{\sqrt{1 + \frac{(1 - x_i - x_j) \Delta^2}{(x_i + x_j) Q^2}}} = \frac{1}{(x_i + x_j) Q^2 \mathbf{r}^2} \sqrt{\frac{x_i x_j}{(x_i + x_j)} Q^2 \mathbf{r}^2} \\ &\times K_1\left(\sqrt{\frac{x_i x_j}{(x_i + x_j)} Q^2 \mathbf{r}^2}\right) + \mathcal{O}(\Delta^2). \end{aligned} \quad (\text{C.44})$$

References

- [1] T. Ahmed et al. (H1), Phys. Lett. B **348**, 681 (1995), [hep-ex/9503005](#).
- [2] C. Adloff et al. (H1), Z. Phys. C **76**, 613 (1997), [hep-ex/9708016](#).
- [3] A. Aktas et al. (H1), Eur. Phys. J. C **48**, 749 (2006), [hep-ex/0606003](#).
- [4] A. Aktas et al. (H1), Eur. Phys. J. C **48**, 715 (2006), [hep-ex/0606004](#).
- [5] F. D. Aaron et al., Eur. Phys. J. C **71**, 1578 (2011), [1010.1476](#).
- [6] F. D. Aaron et al. (H1), Eur. Phys. J. C **72**, 2074 (2012), [1203.4495](#).
- [7] M. Derrick et al. (ZEUS), Z. Phys. C **68**, 569 (1995), [hep-ex/9505010](#).
- [8] J. Breitweg et al. (ZEUS), Eur. Phys. J. C **1**, 81 (1998), [hep-ex/9709021](#).
- [9] J. Breitweg et al. (ZEUS), Eur. Phys. J. C **6**, 43 (1999), [hep-ex/9807010](#).
- [10] S. Chekanov et al. (ZEUS), Nucl. Phys. B **713**, 3 (2005), [hep-ex/0501060](#).
- [11] S. Chekanov et al. (ZEUS), Nucl. Phys. B **816**, 1 (2009), [0812.2003](#).
- [12] S. Chekanov et al. (ZEUS), Eur. Phys. J. C **38**, 43 (2004), [hep-ex/0408009](#).
- [13] F. D. Aaron et al. (H1, ZEUS), Eur. Phys. J. C **72**, 2175 (2012), [1207.4864](#).
- [14] K. J. Golec-Biernat and M. Wusthoff, Phys. Rev. **D59**, 014017 (1998), [hep-ph/9807513](#).
- [15] K. J. Golec-Biernat and M. Wusthoff, Phys. Rev. D **60**, 114023 (1999), [hep-ph/9903358](#).
- [16] A. H. Mueller, Nucl. Phys. B **415**, 373 (1994).
- [17] A. H. Mueller and B. Patel, Nucl. Phys. B **425**, 471 (1994), [hep-ph/9403256](#).
- [18] A. H. Mueller, Nucl. Phys. B **437**, 107 (1995), [hep-ph/9408245](#).
- [19] Z. Chen and A. H. Mueller, Nucl. Phys. B **451**, 579 (1995).
- [20] Y. V. Kovchegov, Phys. Rev. D **60**, 034008 (1999), [hep-ph/9901281](#).
- [21] Y. V. Kovchegov, Phys. Rev. D **61**, 074018 (2000), [hep-ph/9905214](#).
- [22] I. Balitsky, Nucl. Phys. B **463**, 99 (1996), [hep-ph/9509348](#).
- [23] I. Balitsky, Phys. Rev. Lett. **81**, 2024 (1998), [hep-ph/9807434](#).
- [24] I. Balitsky, Phys. Rev. D **60**, 014020 (1999), [hep-ph/9812311](#).
- [25] I. Balitsky, Phys. Lett. B **518**, 235 (2001), [hep-ph/0105334](#).
- [26] J. Jalilian-Marian, A. Kovner, A. Leonidov, and H. Weigert, Nucl. Phys. B **504**, 415 (1997), [hep-ph/9701284](#).
- [27] J. Jalilian-Marian, A. Kovner, A. Leonidov, and H. Weigert, Phys. Rev. D **59**, 014014 (1998), [hep-ph/9706377](#).
- [28] J. Jalilian-Marian, A. Kovner, and H. Weigert, Phys. Rev. D **59**, 014015 (1998), [hep-ph/9709432](#).
- [29] J. Jalilian-Marian, A. Kovner, A. Leonidov, and H. Weigert, Phys. Rev. D **59**, 034007 (1999), [Erratum: Phys.Rev.D 59, 099903 (1999)], [hep-ph/9807462](#).
- [30] A. Kovner, J. G. Milhano, and H. Weigert, Phys. Rev. D **62**, 114005 (2000), [hep-ph/0004014](#).

- [31] H. Weigert, Nucl. Phys. A **703**, 823 (2002), [hep-ph/0004044](#).
- [32] E. Iancu, A. Leonidov, and L. D. McLerran, Nucl. Phys. A **692**, 583 (2001), [hep-ph/0011241](#).
- [33] E. Iancu, A. Leonidov, and L. D. McLerran, Phys. Lett. B **510**, 133 (2001), [hep-ph/0102009](#).
- [34] E. Ferreiro, E. Iancu, A. Leonidov, and L. McLerran, Nucl. Phys. A **703**, 489 (2002), [hep-ph/0109115](#).
- [35] D. Boer et al. (2011), [1108.1713](#).
- [36] Y. V. Kovchegov and H. Weigert, Nucl. Phys. A **784**, 188 (2007), [hep-ph/0609090](#).
- [37] I. Balitsky and G. A. Chirilli, Phys. Rev. D **77**, 014019 (2008), [0710.4330](#).
- [38] I. Balitsky and G. A. Chirilli, Phys. Rev. D **88**, 111501 (2013), [1309.7644](#).
- [39] A. V. Grabovsky, JHEP **09**, 141 (2013), [1307.5414](#).
- [40] I. Balitsky and A. V. Grabovsky, JHEP **01**, 009 (2015), [1405.0443](#).
- [41] A. Kovner, M. Lublinsky, and Y. Mulian, Phys. Rev. D **89**, 061704 (2014), [1310.0378](#).
- [42] M. Lublinsky and Y. Mulian, JHEP **05**, 097 (2017), [1610.03453](#).
- [43] S. Caron-Huot, JHEP **03**, 036 (2018), [1501.03754](#).
- [44] I. Balitsky and G. A. Chirilli, Phys. Rev. D **87**, 014013 (2013), [1207.3844](#).
- [45] G. Beuf, T. Lappi, and R. Paatelainen, Phys. Rev. D **106**, 034013 (2022), [2204.02486](#).
- [46] G. Beuf, H. Hänninen, T. Lappi, Y. Mulian, and H. Mäntysaari, Phys. Rev. D **106**, 094014 (2022), [2206.13161](#).
- [47] G. Beuf, T. Lappi, H. Mäntysaari, R. Paatelainen, and J. Penttala, JHEP **05**, 024 (2024), [2401.17251](#).
- [48] K. Roy and R. Venugopalan, Phys. Rev. D **101**, 034028 (2020), [1911.04530](#).
- [49] P. Caucal, F. Salazar, and R. Venugopalan, JHEP **11**, 222 (2021), [2108.06347](#).
- [50] P. Caucal, F. Salazar, B. Schenke, and R. Venugopalan, JHEP **11**, 169 (2022), [2208.13872](#).
- [51] R. Boussarie, A. V. Grabovsky, L. Szymanowski, and S. Wallon, JHEP **09**, 026 (2014), [1405.7676](#).
- [52] R. Boussarie, A. V. Grabovsky, L. Szymanowski, and S. Wallon, JHEP **11**, 149 (2016), [1606.00419](#).
- [53] P. Taels, T. Altinoluk, G. Beuf, and C. Marquet, JHEP **10**, 184 (2022), [2204.11650](#).
- [54] F. Bergabo and J. Jalilian-Marian, JHEP **01**, 095 (2023), [2210.03208](#).
- [55] F. Bergabo and J. Jalilian-Marian, Phys. Rev. D **106**, 054035 (2022), [2207.03606](#).
- [56] E. Iancu and Y. Mulian (2022), [2211.04837](#).
- [57] P. Caucal and F. Salazar, JHEP **12**, 130 (2024), [2405.19404](#).
- [58] M. Fucilla, A. Grabovsky, E. Li, L. Szymanowski, and S. Wallon, JHEP **02**, 165 (2024), [2310.11066](#).
- [59] M. Fucilla, A. V. Grabovsky, E. Li, L. Szymanowski, and S. Wallon, JHEP **03**, 159 (2023), [2211.05774](#).

- [60] R. Boussarie, A. V. Grabovsky, D. Yu. Ivanov, L. Szymanowski, and S. Wallon, Phys. Rev. Lett. **119**, 072002 (2017), [1612.08026](#).
- [61] H. Mäntysaari and J. Penttala, Phys. Rev. D **105**, 114038 (2022), [2203.16911](#).
- [62] H. Mäntysaari and J. Penttala, JHEP **08**, 247 (2022), [2204.14031](#).
- [63] T. Altinoluk, N. Armesto, G. Beuf, M. Martínez, and C. A. Salgado, JHEP **07**, 068 (2014), [1404.2219](#).
- [64] T. Altinoluk, N. Armesto, G. Beuf, and A. Moscoso, JHEP **01**, 114 (2016), [1505.01400](#).
- [65] T. Altinoluk and A. Dumitru, Phys. Rev. D **94**, 074032 (2016), [1512.00279](#).
- [66] P. Agostini, T. Altinoluk, and N. Armesto, Eur. Phys. J. C **79**, 600 (2019), [1902.04483](#).
- [67] P. Agostini, T. Altinoluk, and N. Armesto, Eur. Phys. J. C **79**, 790 (2019), [1907.03668](#).
- [68] T. Altinoluk, G. Beuf, A. Czajka, and A. Tymowska, Phys. Rev. D **104**, 014019 (2021), [2012.03886](#).
- [69] T. Altinoluk and G. Beuf, Phys. Rev. D **105**, 074026 (2022), [2109.01620](#).
- [70] T. Altinoluk, G. Beuf, A. Czajka, and A. Tymowska, Phys. Rev. D **107**, 074016 (2023), [2212.10484](#).
- [71] T. Altinoluk, N. Armesto, and G. Beuf, Phys. Rev. D **108**, 074023 (2023), [2303.12691](#).
- [72] P. Agostini, T. Altinoluk, and N. Armesto, JHEP **07**, 137 (2024), [2403.04603](#).
- [73] G. A. Chirilli, JHEP **01**, 118 (2019), [1807.11435](#).
- [74] G. A. Chirilli, JHEP **06**, 096 (2021), [2101.12744](#).
- [75] Y. V. Kovchegov, D. Pitonyak, and M. D. Sievert, JHEP **01**, 072 (2016), [Erratum: JHEP 10, 148 (2016)], [1511.06737](#).
- [76] Y. V. Kovchegov, JHEP **03**, 174 (2019), [1901.07453](#).
- [77] F. Cougoulic, Y. V. Kovchegov, A. Tarasov, and Y. Tawabutr, JHEP **07**, 095 (2022), [Erratum: JHEP 09, 052 (2024)], [2204.11898](#).
- [78] T. Altinoluk, G. Beuf, and S. Mulani, Phys. Rev. D **113**, 034011 (2026), [2510.13571](#).
- [79] T. Altinoluk, G. Beuf, J. Favrel, and M. Fucilla (2025), [2512.16788](#).
- [80] R. Boussarie, M. Fucilla, L. Szymanowski, and S. Wallon, Phys. Rev. Lett. **134**, 041901 (2025), [2407.18203](#).
- [81] S. Chekanov et al. (ZEUS), PMC Phys. A **1**, 6 (2007), [0708.1478](#).
- [82] F. Aaron et al. (H1), JHEP **05**, 032 (2010), [0910.5831](#).
- [83] J. Breitweg et al. (ZEUS), Eur. Phys. J. C **14**, 213 (2000), [hep-ex/9910038](#).
- [84] S. Chekanov et al. (ZEUS), Eur. Phys. J. C **26**, 389 (2003), [hep-ex/0205081](#).
- [85] A. Aktas et al. (H1), Phys. Lett. B **638**, 422 (2006), [hep-ex/0603038](#).
- [86] D. Yu. Ivanov and R. Kirschner, Phys. Rev. D **58**, 114026 (1998), [hep-ph/9807324](#).
- [87] D. Y. Ivanov, R. Kirschner, A. Schäfer, and L. Szymanowski, Phys. Lett. B **478**, 101 (2000), [Erratum: Phys.Lett.B 498, 295–295 (2001)], [hep-ph/0001255](#).
- [88] S. Munier, A. M. Stasto, and A. H. Mueller, Nucl. Phys. B **603**, 427 (2001), [hep-ph/0102291](#).

- [89] J. R. Forshaw and G. Poludniowski, *Eur. Phys. J. C* **26**, 411 (2003), [hep-ph/0107068](#).
- [90] R. Enberg, J. R. Forshaw, L. Motyka, and G. Poludniowski, *JHEP* **09**, 008 (2003), [hep-ph/0306232](#).
- [91] G. G. Poludniowski, R. Enberg, J. R. Forshaw, and L. Motyka, *JHEP* **12**, 002 (2003), [hep-ph/0311017](#).
- [92] S. J. Brodsky, L. Frankfurt, J. F. Gunion, A. H. Mueller, and M. Strikman, *Phys. Rev. D* **50**, 3134 (1994), [hep-ph/9402283](#).
- [93] L. Frankfurt, W. Koepf, and M. Strikman, *Phys. Rev. D* **54**, 3194 (1996), [hep-ph/9509311](#).
- [94] J. C. Collins, L. Frankfurt, and M. Strikman, *Phys. Rev. D* **56**, 2982 (1997), [hep-ph/9611433](#).
- [95] A. V. Radyushkin, *Phys. Rev. D* **56**, 5524 (1997), [hep-ph/9704207](#).
- [96] L. Mankiewicz and G. Piller, *Phys. Rev. D* **61**, 074013 (2000), [hep-ph/9905287](#).
- [97] I. V. Anikin and O. V. Teryaev, *Phys. Lett. B* **554**, 51 (2003), [hep-ph/0211028](#).
- [98] H.-n. Li and G. F. Sterman, *Nucl. Phys. B* **381**, 129 (1992).
- [99] M. Vanderhaeghen, P. A. M. Guichon, and M. Guidal, *Phys. Rev. D* **60**, 094017 (1999), [hep-ph/9905372](#).
- [100] S. V. Goloskokov and P. Kroll, *Eur. Phys. J. C* **42**, 281 (2005), [hep-ph/0501242](#).
- [101] S. V. Goloskokov and P. Kroll, *Eur. Phys. J. C* **50**, 829 (2007), [hep-ph/0611290](#).
- [102] S. V. Goloskokov and P. Kroll, *Eur. Phys. J. C* **53**, 367 (2008), [0708.3569](#).
- [103] I. V. Anikin, D. Y. Ivanov, B. Pire, L. Szymanowski, and S. Wallon, *Phys. Lett. B* **682**, 413 (2010), [0903.4797](#).
- [104] I. Anikin, D. Yu. Ivanov, B. Pire, L. Szymanowski, and S. Wallon, *Nucl. Phys. B* **828**, 1 (2010), [0909.4090](#).
- [105] I. Anikin, A. Besse, D. Yu. Ivanov, B. Pire, L. Szymanowski, and S. Wallon, *Phys. Rev. D* **84**, 054004 (2011), [1105.1761](#).
- [106] A. Besse, L. Szymanowski, and S. Wallon, *Nucl. Phys. B* **867**, 19 (2013), [1204.2281](#).
- [107] A. Besse, L. Szymanowski, and S. Wallon, *JHEP* **11**, 062 (2013), [1302.1766](#).
- [108] A. D. Bolognino, F. G. Celiberto, D. Yu. Ivanov, and A. Papa, *Eur. Phys. J. C* **78**, 1023 (2018), [1808.02395](#).
- [109] A. D. Bolognino, A. Szczurek, and W. Schaefer, *Phys. Rev. D* **101**, 054041 (2020), [1912.06507](#).
- [110] A. D. Bolognino, F. G. Celiberto, D. Yu. Ivanov, A. Papa, W. Schäfer, and A. Szczurek, *Eur. Phys. J. C* **81**, 846 (2021), [2107.13415](#).
- [111] I. P. Ivanov and N. N. Nikolaev, *Phys. Rev. D* **65**, 054004 (2002), [hep-ph/0004206](#).
- [112] M. Hentschinski, A. Sabio Vera, and C. Salas, *Phys. Rev. Lett.* **110**, 041601 (2013), [1209.1353](#).
- [113] K. J. Golec-Biernat and M. Wusthoff, *Phys. Rev. D* **59**, 014017 (1998), [hep-ph/9807513](#).
- [114] G. Watt, A. Martin, and M. Ryskin, *Eur. Phys. J. C* **31**, 73 (2003), [hep-ph/0306169](#).
- [115] G. R. Boroun, *Eur. Phys. J. C* **84**, 960 (2024), [2407.02800](#).

- [116] G. R. Boroun, P. Ha, A. V. Kotikov, and A. V. Lipatov (2025), [2510.14678](#).
- [117] R. Boussarie, M. Fucilla, L. Szymanowski, and S. Wallon, Phys. Rev. D **111**, 014032 (2025), [2407.18115](#).
- [118] L. D. McLerran and R. Venugopalan, Phys. Rev. D **49**, 3352 (1994), [hep-ph/9311205](#).
- [119] L. D. McLerran and R. Venugopalan, Phys. Rev. D **49**, 2233 (1994), [hep-ph/9309289](#).
- [120] L. D. McLerran and R. Venugopalan, Phys. Rev. D **50**, 2225 (1994), [hep-ph/9402335](#).
- [121] A. Airapetian et al. (HERMES), Eur. Phys. J. C **71**, 1609 (2011), [1012.3676](#).
- [122] F. Cougoulic, P. Korcyl, and T. Stebel, Comput. Phys. Commun. **313**, 109616 (2025), [2411.12739](#).
- [123] B. Ducloué, E. Iancu, A. H. Mueller, G. Soyez, and D. N. Triantafyllopoulos, JHEP **04**, 081 (2019), [1902.06637](#).
- [124] T. Lappi and H. Mäntysaari, Phys. Rev. D **88**, 114020 (2013), [1309.6963](#).
- [125] P. Ball, V. M. Braun, Y. Koike, and K. Tanaka, Nucl. Phys. B **529**, 323 (1998), [hep-ph/9802299](#).
- [126] D. Becirevic, P. Boucaud, L. Giusti, J. P. Leroy, V. Lubicz, G. Martinelli, F. Mescia, and F. Rapuano (1998), [hep-lat/9809129](#).
- [127] D. Yu. Ivanov, M. I. Kotsky, and A. Papa, Eur. Phys. J. C **38**, 195 (2004), [hep-ph/0405297](#).